BMC Genomics

RESEARCH Open Access

Single-cell RNA and DNA methylome profiling reveal liquid helium vitrification enhances porcine parthenogenetically activated blastocyst viability

Jesse Oluwaseun Ayantoye[1†], Baigao Yang[1†], Jianhua Dong[1], Xiaoyi Feng[1], Muhammad Shahzad[1], Hubdar Ali Kolachi[1], Pengcheng Wan[2], Hongmei Pan[3*] and Xueming Zhao[1,2*]

Abstract

Background Cryopreservation of porcine blastocysts remains a significant challenge due to their high lipid content, which can lead to cryoinjury and reduced developmental competence. While liquid nitrogen (LN) vitrification causes significant molecular damage, LHe vitrification enhances oocyte viability, reduces cryoinjury, and better preserves ultrastructure and gene expression. Despite these advantages, the specific effects of LHe vitrification on porcine blastocysts are still underexplored.

Results LHe vitrification significantly improved post-thaw survival rates (96.53 ± 4.27%) compared to conventional LN (71.20 ± 6.82%) and modified LN protocols (90.77 ± 7.88%). scRNA-seq and scWGBS achieved mapping rates of 83.70% and 33.69%, respectively, and a bisulfite conversion efficiency of 99.27%, ensuring high-quality data for gene expression and methylation analysis. Vitrification significantly altered gene expression and epigenetic regulation, with hypermethylation and downregulation of genes associated with energy metabolism (*ARG2*, *AUH*, *IDH3A*, *NDUFV1*), immune function (*CD53*), and protein processing (*B4GALT5*, *OSTC*, *DPM3*, *EXT1*), resulting in mitochondrial and immune dysfunction, as well as protein instability. KEGG pathway analysis revealed disruptions in the TCA cycle, pentose phosphate pathway, homologous recombination, and fatty acid biosynthesis, which impaired blastocyst viability, ATP availability, immune responses, and cellular communication. Conversely, hypomethylation and upregulation of genes regulating energy metabolism (*GPAM*, *AICDA*), oxidative stress response (*ITGAV*), and cell adhesion (*PLAU*, *MRAP2*) suggest an adaptive response to mitigate cellular stress and damage. However, excessive upregulation following vitrification may lead to metabolic strain, oxidative stress accumulation, lipotoxicity, and an increased risk of apoptosis.

†Jesse Oluwaseun Ayantoye and Baigao Yang contributed equally to this work.

*Correspondence:
Hongmei Pan
panhm_2118@163.com
Xueming Zhao
zhaoxueming@caas.cn

Full list of author information is available at the end of the article

© The Author(s) 2026. **Open Access** This article is licensed under a Creative Commons Attribution-NonCommercial-NoDerivatives 4.0 International License, which permits any non-commercial use, sharing, distribution and reproduction in any medium or format, as long as you give appropriate credit to the original author(s) and the source, provide a link to the Creative Commons licence, and indicate if you modified the licensed material. You do not have permission under this licence to share adapted material derived from this article or parts of it. The images or other third party material in this article are included in the article's Creative Commons licence, unless indicated otherwise in a credit line to the material. If material is not included in the article's Creative Commons licence and your intended use is not permitted by statutory regulation or exceeds the permitted use, you will need to obtain permission directly from the copyright holder. To view a copy of this licence, visit http://creativecommons.org/licenses/by-nc-nd/4.0/.

Conclusions Our findings demonstrate that LHe offers superior metabolic and epigenetic preservation compared to LN, thereby reducing molecular damage and enhancing post-thaw development. These results establish LHe vitrification as an effective method that increases blastocyst viability and reproductive biotechnology applications.

Keywords Vitrification, Porcine blastocyst, Single-cell sequencing, DNA methylation, Cryopreservation

Background

Cryopreservation of oocytes, blastocysts, embryos, and gametes plays a pivotal role in preserving genetic resources, supporting efficient breeding programs, and advancing reproductive biotechnology [1]. However, the cryopreservation of porcine embryos, particularly blastocysts, presents significant challenges due to their high lipid content, which increases their susceptibility to cryoinjury and low-temperature damage. This characteristic leads to ice crystal formation during freezing, disrupting cellular structures and contributing to poor cryopreservation success rates [2, 3]. Therefore, improved cryopreservation strategies are urgently needed to enhance the survival and developmental competence of porcine blastocysts, thereby optimizing the efficiency of breeding and genetic enhancement programs.

Vitrification has emerged as a superior alternative to traditional freezing methods due to its ability to effectively prevent ice crystal formation by rapidly cooling cells without freezing [4]. By employing ultrafast cooling rates and high concentrations of cryoprotectants, vitrification transforms biological samples into a glass-like state, thereby maintaining the biological integrity of embryos. This technique has significantly improved cryopreservation outcomes, particularly for porcine embryos [2]. However, the high concentration and composition of permeating cryoprotectants can influence post-warming embryo survival and developmental competence [5]. Furthermore, despite its advantages, vitrified porcine blastocysts, particularly those frozen with liquid nitrogen (LN), show suboptimal developmental competence when compared to in vivo-derived embryos and those from other model organisms, such as mice and cattle [6, 7]. Due to the limitations of LN, alternative cryogenic agents, such as Liquid Helium (LHe), have gained attention in reproductive biotechnology to optimize vitrification conditions.

LHe serves as a promising modification to vitrification, functioning as an ultra-rapid cryogenic cooling agent [8]. LHe vitrification improves oocyte viability, mitigates cryoinjury, and preserves ultrastructure and gene expression better than LN, leading to reduced cryodamage, higher survival rates, and enhanced post-thaw developmental competence [9]. Similarly, LHe achieves ultra-rapid cooling rates, minimizing intracellular ice formation and oxidative stress, thereby enhancing cryopreservation efficiency compared to LN [10]. LHe vitrification can potentially reduce cryoinjury and preserve embryos' epigenetic and transcriptional integrity, which could lead to enhanced survival and developmental outcomes [11]. While LHe vitrification has demonstrated promising results in bovine oocyte cryopreservation, its effects on porcine embryos, particularly parthenogenetically activated blastocysts, remain largely unexplored. Further research is needed to determine whether LHe vitrification can enhance porcine blastocyst survival and developmental outcomes.

Despite advancements in vitrification techniques, challenges persist in preserving genomic stability, mitochondrial function, and regulating apoptosis post-cryopreservation [12]. Addressing these challenges requires a deeper understanding of the molecular mechanisms underlying the alterations induced by vitrification. Recent advances in sequencing technologies, such as RNA sequencing (RNA-seq) and DNA methylation analysis, have the potential to investigate the molecular effects of cryopreservation at both the transcriptional and epigenetic levels [13]. RNA-seq plays a pivotal role in elucidating how vitrification affects gene expression, shedding light on molecular pathways that may impact developmental quality [14]. Similarly, DNA methylation studies reveal how cryopreservation affects the epigenome, influencing embryo viability and developmental potential [15].

Recent studies have investigated the effects of vitrification on the transcriptome profile of porcine embryos, including both in vitro-produced and in vivo-derived blastocysts [16–19]. Almiñana et al. (2022) [16] demonstrated that vitrification induces changes in gene expression in porcine blastocysts, reflecting both cryodamage and the embryo's repair processes, which could impact embryo viability and post-transfer development. Similarly, Wiesak and Goryszewska-Szczurek (2022) [18] reported modifications in specific gene expressions that may affect the embryos' developmental trajectory. In another study, Jia et al. (2024) [17] highlighted that the vitrification of porcine germinal vesicle oocytes can alter gene expression patterns during subsequent embryonic stages, potentially affecting developmental competence. Importantly, transcriptomic analyses of in vivo-derived porcine embryos have also shown that vitrification alters genes involved in metabolism, cell cycle regulation, stress response, and key signaling pathways such as TGF-β, MAPK, and p53, indicating that cryopreservation-induced molecular perturbations also occur under physiological conditions [19]. However, these studies are limited to transcriptomic analyses of in vitro and

in vivo-derived oocytes, leaving a critical gap in understanding how vitrification affects both the epigenetic modifications and gene expression in parthenogenetically activated (PA) porcine blastocysts. This gap is particularly significant as porcine parthenogenetically activated (PA) blastocysts offer a well-established model for evaluating cytoplasmic maturation and developmental competence in vitro [20], and thus provide a robust system for investigating developmental mechanisms and optimizing cryopreservation strategies.

Therefore, this study aims to fill this gap by introducing LHe vitrification as a novel approach to enhance the cryopreservation of porcine blastocysts. We aim to investigate the molecular effects of LHe vitrification on parthenogenetically activated porcine blastocysts by examining transcriptional and epigenetic changes using advanced single-cell RNA sequencing (scRNA-seq) and single-cell whole-genome bisulfite sequencing (scWGBS). We aim to identify molecular differences between non-vitrified, LN-vitrified, and LHe-vitrified blastocysts, thereby elucidating the mechanisms that influence developmental competence and advancing cryopreservation strategies to improve porcine blastocyst viability.

Materials and methods

Porcine oocytes collection

Porcine ovaries were collected from a nearby slaughterhouse and transported to the laboratory at a temperature of 35–37 °C within 2 h in a 0.9% saline solution containing penicillin (100 UI/mL) and streptomycin (10 mg/mL). Cumulus–oocyte complexes (COCs) were aspirated from the ovaries using a disposable syringe with an 18-gauge needle from follicles 3 to 8 mm in diameter. The COCs were washed in manipulation media (TCM-199 HEPES-buffered medium supplemented with 1% pFF), and suitable COCs with at least three compact layers of cumulus cells and homogeneous cytoplasm were selected for IVM.

In Vitro maturation of the oocytes

Oocytes were matured in vitro according to [21], with slight modifications. COCs were matured at 37 °C in 5% CO_2 in a maturation medium for 44 h containing TCM 199 supplemented with 40 ng/mL of Fibroblast Growth Factor 2 (FGF2), 20 ng/mL of Insulin-like Growth Factor 1, 20 ng/mL of Leukaemia Inhibitory Factor, 20% pFF, 1 mM dibutyryl cyclic adenosine monophosphate (dbcAMP), 2 mM of Pyruvate, 5.6 mM of Glucose, 0.5 UI/mL hCG, 0.5 UI/mL FSH and 50 mM of Nicotinamide (NAM). Twenty oocytes were cultured in 100 µL of IVM medium under mineral oil.

After maturation, the cumulus cells were removed from the oocytes by vortexing for 4 min in Tyrode lactate-Hepes (TL-Hepes), which was supplemented with 0.1% PVA and 0.1% hyaluronidase. Denuded oocytes with a visible polar body were selected in the oocyte manipulation medium.

Parthenogenetic activation (PA) of the oocytes

Parthenogenetic activation was performed on mature oocytes, as described by [22], with slight modifications. Matured oocytes were washed 3 times in activation medium (0.1 mg/mL PVA, 0.3 M mannitol, 0.1 mM CaCl2·2H2O, 0.5 mM MgCl2·6H2O, 0.8 mM HEPES). The mature oocytes were arranged sequentially in the electrophoresis tank, and two continuous DC pulses of 1.2 kV/cm were activated by the ECM2001 electrofusion instrument (ECM2001, BTX, USA) for 30 µs. After activation, the oocytes were washed. Subsequently, the blastocysts were transferred to culture medium PZM-3 and cultured at 38.5 °C with 5% CO2 for 6 days, during which they developed into blastocysts.

Vitrification and thawing of the blastocysts

The 6-day PA blastocysts were divided into four groups: fresh control (AA), LN-vitrified (BB), modified LN-vitrified (CC), and LHe-vitrified (HH). The 6-day PA blastocysts (Groups BB and CC with some treatment) were subjected to the vitrification method (Cryotop Vitrification) according to [23], with slight modifications.

For group BB vitrification, the blastocysts were equilibrated in vitrification solution I (PZM-3 containing 7.5% ethylene glycol (EG), 7.5% dimethyl sulfoxide (DMSO), and 20% fetal bovine serum (FBS)) for 5 min. They were then transferred to vitrification solution II (PZM-3 containing 0.4 mol/L sucrose, 15% EG, 15% DMSO, and 20% FBS) for 30 s. Subsequently, 3–5 blastocysts were loaded onto a single Cryotop device using a minimal volume of vitrification solution and quickly immersed in liquid nitrogen for cryopreservation.

For group CC vitrification, the blastocysts were equilibrated in vitrification solution I (PZM-3 containing 7.5% ethylene glycol (EG), 7.5% dimethyl sulfoxide (DMSO), and 20% fetal bovine serum (FBS)) and supplemented with 7.5 mg/mL cytochalasin B for 5 min. They were then transferred to vitrification solution II (PZM-3 containing 0.4 mol/L sucrose, 15% EG, 15% DMSO, 1% nanoparticles Fe_3O_4, 7.5 mg/mL cytochalasin-b, and 20% FBS) for 30 s. Subsequently, 3–5 blastocysts were loaded onto a single Cryotop device using a minimal volume of vitrification solution and quickly immersed in liquid nitrogen for cryopreservation.

For group HH vitrification, vitrification followed the same protocol as LN vitrification, except that Cryotops were initially plunged into liquid helium (LHe) prior to transfer into liquid nitrogen (LN) according to [9], with slight modifications. Briefly, 3–5 blastocysts were loaded onto a single Cryotop device using minimal vitrification solution, attached to the aluminum wire with tape,

and immediately transferred into LHe. For plunging, the insertion of the aluminum wire was stopped when a large amount of gas was emitted from the LHe. The Cryotop with blastocysts was held in LHe for a few seconds until the gas emissions stabilized. The Cryotop was then moved from the LHe to the LN container by grasping the aluminum wire as quickly as possible. The time interval between contact with the vitrification solution and cooling did not exceed 30 s, and the interval between removing the Cryotop from LHe and plunging it into LN did not exceed 3 s. Finally, the Cryotop was detached from the aluminum wire and stored in LN.

For thaw, the Cryotop slide containing the blastocysts was immersed in a preheated thawing solution I (PZM-3 containing 0.3 mol/L sucrose and 20% FBS) at 37 °C and gently agitated to facilitate the detachment of the blastocysts from the slide. After equilibrating for 3 min, the blastocysts were transferred to thawing solution II (PZM-3 containing 0.15 mol/L sucrose and 20% fetal bovine serum (FBS)) at 37 °C for an additional 3 min. The blastocysts were washed thrice with PZM-3 and cultured in fresh PZM-3 for 24 h. The vitrified blastocysts were stored in LN for 24 h before thawing. Only those with good morphological recovery were selected for single-cell transcriptome sequencing.

Assessment of the vitrified blastocysts

After thawing for 24 h, the state of the vitrified blastocysts was evaluated by morphological observation under a stereomicroscope, according to [24], with a few modifications. Those with intact morphology were selected for subsequent experiments. The collected blastocysts were placed in a lysis buffer for single-cell sequencing and stored at -80 °C.

Survival rates were calculated as the percentage of morphologically intact blastocysts among those evaluated post-thaw. A statistical comparison of survival rates among groups was performed using one-way ANOVA, followed by Tukey's post-hoc test, with $P < 0.05$ considered statistically significant.

Single blastocyst preparation for transcriptome and methylome analysis

For both single-cell RNA and DNA methylation sequencing, each porcine blastocyst was treated as a single biological replicate for every experimental group. Each blastocyst was carefully selected under a microscope, thoroughly washed in PBS, and transferred into a separate 200 µL PCR tube for lysis. Cytoplasmic RNA and nuclear DNA were simultaneously extracted from the same lysate using a magnetic bead-based separation method, enabling parallel processing of the transcriptome and methylome. Cytoplasmic RNA was used for single-cell transcriptome profiling, while nuclear DNA was processed for whole-genome bisulfite sequencing to assess DNA methylation patterns.

Single-cell RNA sequencing

Smart-Seq2 scRNA-Seq was performed using the protocol described by [25], with slight modifications. Briefly, single cells were sorted into cell lysis buffer containing 0.1 µL RNase inhibitor (Clontech), 1.9 µL Triton X-100 solution (1%), 1 µL dNTP mix (10 mM), and 1 µL oligo-dT primer (5 µM). Reverse transcription was performed containing 0.5 µL SuperScript II reverse transcriptase (200 U/µL, Invitrogen), 0.25 µL RNase inhibitor (40 U/µL, Clontech), 2 µL Superscript II First-Strand Buffer (5×, Invitrogen), 0.5 µL DTT (0.1 M, Invitrogen), 2 µL Betain (5 M, Sigma), 0.06 µL MgCl2 (1 M, Sigma), 0.1 µL TSO (100 µM). Reverse transcription was carried out at 25 °C for 5 min, then at 42 °C for 60 min, then at 50 °C for 30 min, and finally at 72 °C for 10 min. PCR preamplification was performed using KAPA HiFi HotStart Ready MIX (KAPA Biosystems) with 22 cycles of PCR and the IS PCR primer reduced to 50 nM (4 cycles at 98 °C for 20 s, 65 °C for 30 s, and 72 °C for 5 min, followed by 18 cycles at 98 °C for 20 s, 67 °C for 15 s, and 72 °C for 5 min, with a final cycle at 72 °C for 5 min.). Subsequently, Amplified samples were purified twice with 0.8X Ampure XP beads (Beckman, A63882). We constructed a library from enriched cDNA fragments attached to C1 beads using KAPA Hyper Prep Kits (KK8504). We used the NEB U-shape adaptor for ligation. Libraries were sequenced to generate 150-bp paired-end reads on an Illumina Novaseq 6000 platform.

Single-cell whole-genome DNA methylation sequencing

Whole-genome bisulfite sequencing (WGBS) steps were used to amplify the single-cell methylome, as described by [26] with some modifications. Briefly, single cells were sorted into a cell lysis buffer containing 20 mM Tris–EDTA [pH 8.0], 20 mM KCl, and 0.3% Triton X-100, along with 1 mg/mL protease (Qiagen) and 60 fg unmethylated lambda DNA (Fermentas). Lastly, the total volume was adjusted to 4.5 µL with nuclease-free water. The cells were then lysed for 3 h at 50 °C and heat-inactivated for 30 min at 75 °C.

Bisulfite conversion was performed in a 150 µL reaction (125 µL CT conversion reagent, 20 µL Nuclease-free water, and 5 µL single cell lysate) using the EZ-96 DNA Methylation-Direct™ MagPrep kit (Invitrogen) following the manufacturer's standard protocol. First, the double-stranded DNA was denatured for 8 min at 98 °C; then, the reaction was incubated for 3.5 h at 64 °C to ensure complete bisulfite conversion. All these steps were performed in a PCR thermocycler. After this step, the converted DNA was purified using Zymo-Spin columns (Zymo) with 10 ng tRNA (Roche) as a carrier; the

DNA was finally eluted in 20 mL of elution buffer. The purified DNA was subjected to two rounds of amplification in 24 μL reactions using bisulfite-converted DNA (19.5 μL), 10 × Blue Buffer (2.5 μL), and 10 μM oligo1 primer ((Biotin) CTACACGACGCTCTTCCGATCTNNNNNNNNN) (1 μL). It was incubated at 65 °C for 3 min, followed by a 4 °C pause. Next, 50 U of Klenow exo-(NEB) were added, and the samples were incubated at 4 °C for 5 min, then warmed to 37 °C at a rate of + 1 °C per 15 s and held at 37 °C for 30 min. This random priming and extension were repeated 3 times (10 rounds). The samples were incubated with 20 U of exonuclease I (NEB) for 1 h at 37 °C before purifying the DNA using 0.8 × Ampure XP beads (Beckman Clulter). The beads were eluted in 39 μL of QIAGEN EB according to the manufacturer's guidelines.

Samples were eluted in 10 μM oligo2 (TGCTGAACCGCTCTTCCGATCTNNNNNNNNN), 10 mM dNTP, and 10 × Blue buffer and incubated at 95 °C for 45 s. They were then immediately transferred to ice, then added 50 U of Klenow exo-(NEB) and incubated at 4 °C for 5 min, followed by a temperature increase of 1 °C every 15 s until reaching 37 °C, where they were held for 90 min. DNA was purified using 0.9 × Ampure XP beads (Beckman Coulter), and the beads were then eluted in 23 μL of QIAGEN EB according to the manufacturer's guidelines.

The 23 μL DNA samples were supplemented with 15 μM Universal PCR Primer (NEB), 15 μM Index Primer (NEB), and 2 × Kapa HiFi Mix. Libraries were then amplified using PCR as follows: 95 °C for 2 min, followed by 13–14 repeats of (94 °C for 80 s, 65 °C for 30 s, 72 °C for 30 s), and then 72 °C for 3 min, with a final hold at 4 °C. Amplified libraries were purified using 0.8 × Ampure XP beads (Beckman Clulter) twice, final elute with 30 μL NF-H_2O, and were assessed for quality and quantity using High-Sensitivity DNA chips on the Agilent Bioanalyser and the KAPA Library Quantification Kit for Illumina (KAPA Biosystems). The final quality-ensured libraries were used for pair-ended deep sequencing on an Illumina HiSeqX-ten Sequencer, and all clusters that passed the filter were converted into FASTQ files using a standard Illumina pipeline.

Data quality, filtering, and analysis

Raw RNA-seq reads were filtered using FastQC to remove adapter sequences, low-quality bases, and contaminants. The filtered sequences were aligned to the reference genome (Suscrofa11.1) using Tophat (version 2.0.13). Cufflinks (version 2.2.1) was used to normalize and verify the gene expression level between two samples. DESeq2 was used to analyze the differences in gene count matrices of duplicate samples within a group. Genes were considered significantly differentially expressed if they had an adjusted p-value < 0.05 and an absolute $\log_2$ fold change ($|\log_2 FC| \geq 1.2$. All fold-change values reported in this study are $\log_2 FC$.

Raw DNA methylation sequencing reads were filtered using FastQC to remove adapters, low-quality bases, and contaminating sequences. The filtered DNA methylation sequences were then compared with the reference genome (Suscrofa11.1) using the bs_seeker2-align.py tool in BS_seeker2 (v2.1.1). The paired-end sequencing data were compared separately. The bs_seeker2- call_methyl.py tool in bs_seeker2 (v2.1.1) was used to detect methylation sites and amounts, with significance thresholds set at a q-value < 0.05 and a minimum methylation difference of 20% between groups.

Gene Ontology (GO) and Kyoto Encyclopaedia of Genes and Genomes (KEGG) enrichment

The Differentially Expressed Genes (DEGs) and Differentially Methylated Regions (DMRs) were then subjected to GO and KEGG analyses to classify genes and identify functional enrichment. GO was analyzed using TopGO (version 2.24.0), and KEGG was analyzed using the ontology-based tool clusterProfiler (version 4.6.1). GO and KEGG analyses were performed using the RNA-seq DEGs and DNA methylation DMRs, with promoter regions and genes analyzed separately.

GO and KEGG enrichment analyses were conducted to explore the biological functions of the interactions between DEGs and DMRs, categorized into hypermethylated and downregulated genes (DNA methylation detamC > 0.2, P-value < 0.01; RNAseq Foldchange < -2, P-value < 0.01) and hypomethylated and upregulated genes (DNA methylation detamC < 0.2, P-value < 0.01; RNAseq Foldchange > 2, *P*-value < 0.01). From the set of significantly enriched pathways, representative genes and corresponding methylation regions were selected to illustrate the coordinated transcriptional and epigenetic patterns identified in the interaction analysis.

Experimental design

The experimental samples were divided into four groups based on vitrification conditions, with three replicates for each group except for Group BB, which had two replicates. Group AA (A1, A2, and A3) consisted of fresh (non-vitrified) porcine blastocysts and served as the control group. Group BB (B1 and B2) included porcine blastocysts vitrified in LN. Group CC (C1, C2, and C3) comprised vitrified porcine blastocysts treated with a modified LN vitrification protocol. Group HH (H1, H2, and H3) included vitrified porcine blastocysts using LHe. Following vitrification and thawing, morphologically intact blastocysts were selected for downstream molecular analysis. Each blastocyst was processed individually for parallel transcriptomic and methylomic profiling. Cytoplasmic RNA and nuclear DNA were simultaneously

extracted from the same blastocyst lysate for Smart-seq2-based scRNA-seq and single-cell whole-genome bisulfite sequencing (scWGBS), respectively. Differential gene expression and methylation analyses were performed between groups, followed by integrated DEG–DMR analysis and GO/KEGG enrichment to assess functional and pathway alterations associated with vitrification strategies.

Results

Blastocysts survival assessment and statistical summary

Table 1 presents a summary of blastocyst survival outcomes following vitrification and post-thaw assessment across three treatment groups. The survival analysis shows that the vitrification protocol significantly influenced post-thaw blastocyst viability. The HH group exhibited the highest survival rate, followed by the CC group, while the BB group showed the lowest survival outcome. Statistical analysis confirmed significant differences between all groups, as indicated by distinct superscript letters.

Effect of vitrification on transcription profile of porcine parthenogenetic blastocysts

Single-cell RNA sequencing was performed to assess transcriptional differences among fresh (AA), LN-vitrified (BB), modified LN-vitrified (CC), and LHe-vitrified (HH) blastocysts. Pairwise comparisons were conducted to identify differentially expressed genes (DEGs) across treatment groups. Sequencing quality metrics showed Q20 and Q30 values above 96% across all samples, with an average mapping rate of 83.70% to the Sus scrofa 11.1 reference genome (Supplementary Table S1).

Analysis of Differentially Expressed Genes (DEGs)

Differential expression analysis revealed substantial transcriptional variation across the six pairwise comparisons (Fig. 1A–B). The number of DEGs ranged from 2,596 in CC vs BB to 4,514 in HH vs CC. Comparisons involving the HH group showed higher DEG counts relative to LN-based contrasts. Both upregulated and downregulated genes were detected in all comparisons. The differential gene bar chart (Fig. 1A) summarizes the magnitude and direction of DEGs across comparisons. In contrast, the volcano plots (Fig. 1B) illustrate the distribution of significantly altered genes based on $\log_2$ fold change and adjusted p-value thresholds.

Table 1 Summary of blastocysts vitrification, assessment, and survival rates across vitrified groups

Group	Number of Blastocysts Vitrified (n)	Number of Blastocysts Assessed Post-Thaw (n)	Number of Embryos Survived (n)	Survival Rate (%)
BB	125	125	89	71.20 ± 6.82^{c}
CC	130	130	118	90.77 ± 7.88^{b}
HH	144	144	139	96.53 ± 4.27^{a}

Values are presented as mean ± SE from three independent biological replicates. Different superscript letters within a column indicate significant differences ($P < 0.05$)

Gene classification and functional enrichment analysis of DEGs

Figure 2 presents the GO enrichments for DEGs across group comparisons. Vitrification altered a wide range of biological processes (BP), molecular functions (MF), and cellular components (CC), with marked differences between fresh and vitrified groups. Blastocysts vitrified using LN, particularly in the BB and CC groups, exhibited enrichment of GO terms linked to mitochondrial dysfunction, RNA binding, and disrupted biosynthetic activity. In contrast, blastocysts vitrified with LHe (HH group) showed distinct enrichment in processes such as protein transport, oxidoreductase activity, and organelle-associated functions. The KEGG pathway analysis (Fig. 3) further identifies several key pathways that differ across groups, including oxidative phosphorylation, the tricarboxylic acid (TCA) cycle, and protein processing in the endoplasmic reticulum.

Effect of vitrification on DNA methylation sequencing analysis of porcine parthenogenetic blastocysts

Single-cell whole-genome bisulfite sequencing (scWGBS) was performed to assess DNA methylation differences among AA, BB, CC, and HH blastocysts. Differentially methylated regions (DMRs) were identified through pairwise comparisons between treatment groups. Promoter and gene-body methylation patterns were analyzed, followed by functional enrichment analysis of associated genes. The average bisulfite conversion efficiency was 99.27%, with an average mapping rate of 33.69% across samples (Supplementary Table S2).

Analysis of Differentially Methylated Regions (DMRs)

Differentially methylated regions (DMRs) were identified across all pairwise comparisons. Both shared and comparison-specific DMRs were detected (Fig. 4). Comparisons involving the HH group contained more unique DMRs than LN-based contrasts. The BB vs AA comparison showed fewer unique DMRs and greater overlap with other LN-related contrasts. The distribution of shared and unique DMRs across comparisons is presented in Fig. 4.

Gene classification and functional enrichment analysis of DMRs

GO enrichment analysis of DMR-associated genes identified functional categories across biological process, molecular function, and cellular component domains

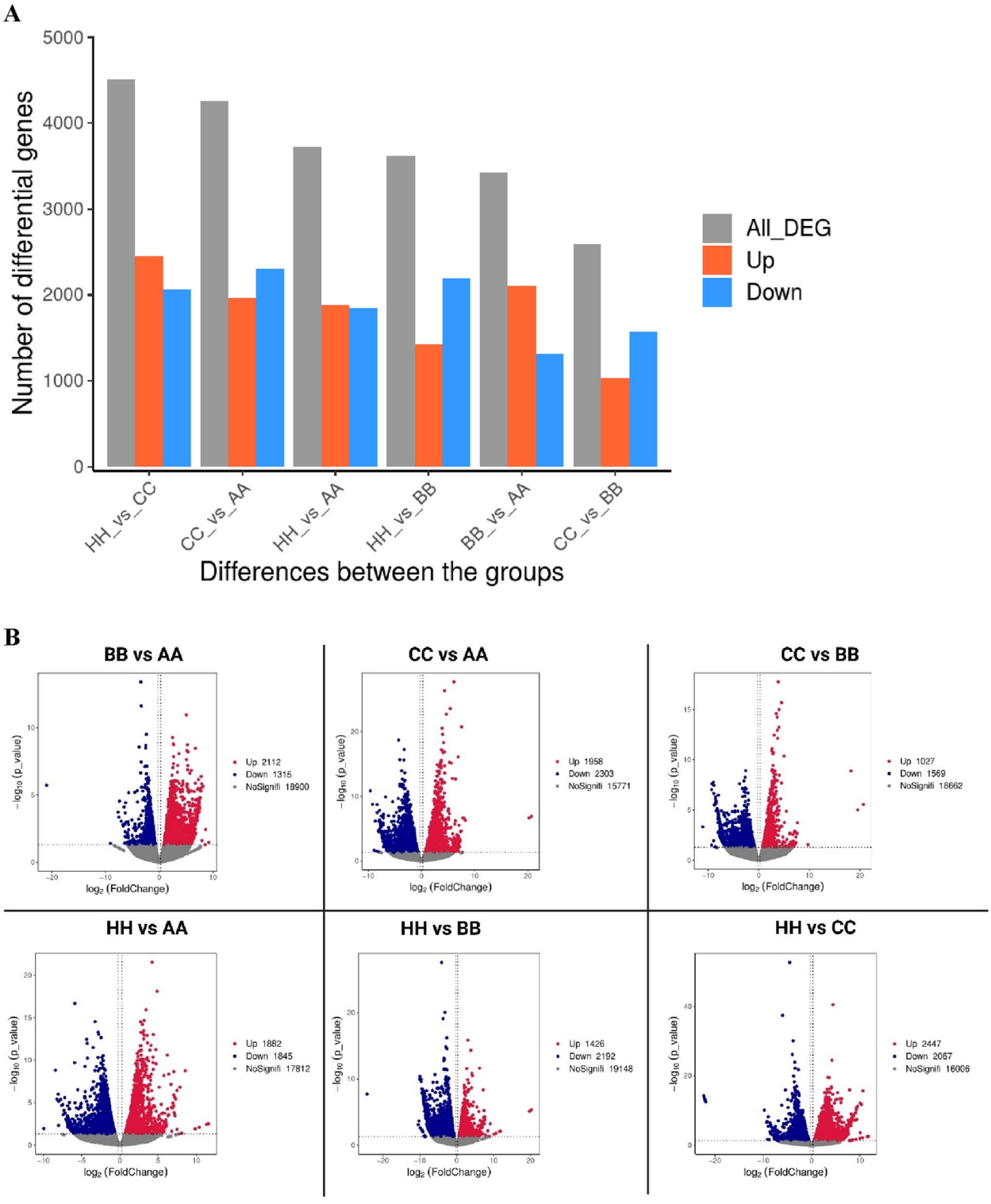

Fig. 1 Differential Expression Analysis of Genes in the sample. **A** Differential gene bar chart. **B** Volcano Plots of DEGs in the sample comparison of BB vs. AA, CC vs. AA, CC vs. BB, HH vs. AA, HH vs. BB, and HH vs. CC

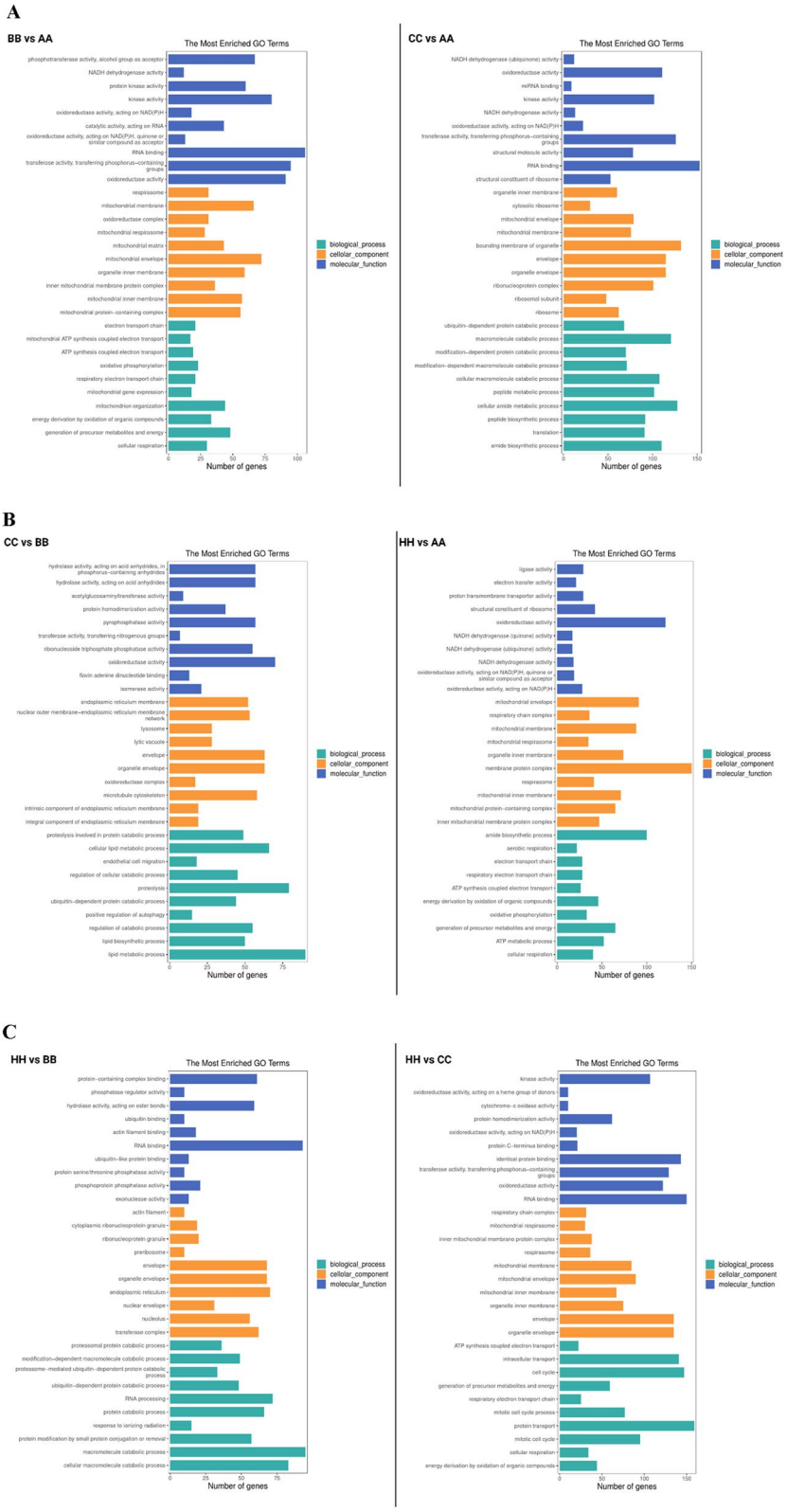

Fig. 2 GO terms in DEGs. **A** BB vs AA and CC vs AA. **B** CC vs BB and HH vs AA. **C** HH vs BB and HH vs CC

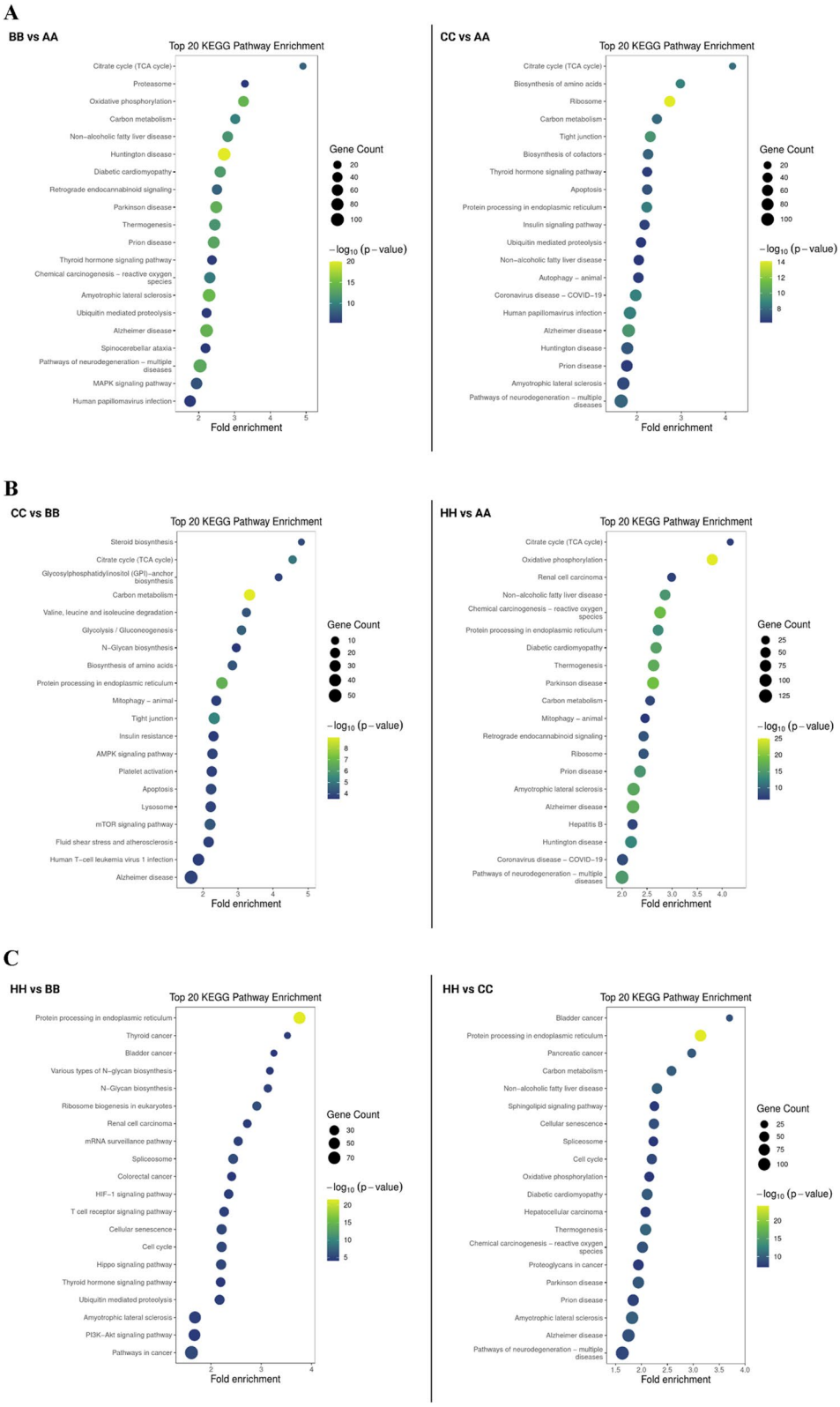

Fig. 3 KEGG pathway analysis of DEGs. **A** BB vs AA and CC vs AA. **B** CC vs BB and HH vs AA. **C** HH vs BB and HH vs CC

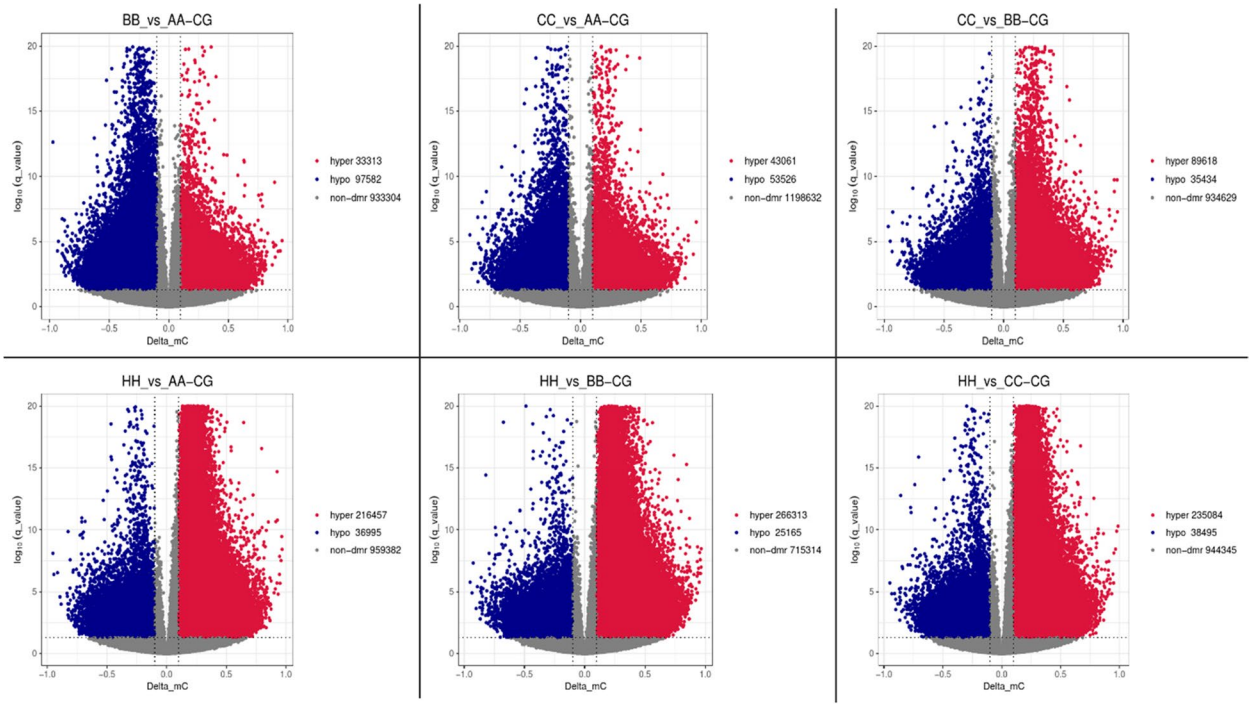

Fig. 4 Charts of Differentially Methylated Regions Between Groups: DMR volcano plot of BB vs. AA, CC vs. AA, CC vs. BB, HH vs. AA, HH vs. BB, and HH vs. CC in the CG context

(Fig. 5). In BB vs AA comparisons, enriched terms included ion transport and transmembrane activity. In CC vs AA and CC vs BB comparisons, enriched categories included metabolic regulation, extracellular organelle functions, and cell differentiation. In HH-related comparisons (HH vs AA, HH vs BB, HH vs CC), enriched terms included epithelial development, kinase signaling, vesicle-mediated transport, and cellular response processes.

The KEGG pathway analysis (Fig. 6) identified several key pathways that are significantly enriched across group comparisons. LN-vitrified blastocysts predominantly impacted amino acid metabolism pathways (e.g., histidine, arginine, and proline metabolism). Modified LN-vitrified (CC) blastocysts showed enrichments in pathways related to longevity regulation, immune signaling, and cardiomyopathy pathways. Notably, LHe vitrification (HH) comparisons showed enrichment in pathways including phototransduction, gastric secretion, cortisol synthesis, diabetes-related pathways, and platelet activation.

Gene classification and functional enrichment analysis of the interaction of DEGs and DMRs

To investigate coordinated epigenetic and transcriptional regulation, we analyzed the interaction between differentially expressed genes and promoter-associated DMRs. This integrative approach identified genes exhibiting statistically significant changes in both expression and promoter methylation. From this interaction analysis, selected upregulated and downregulated genes are presented in Table 2, while the corresponding methylation changes for these interacting genes are summarized in Table 3. Across the comparisons, these genes (Table 2) were annotated to pathways related to energy metabolism, cellular signaling, glycosylation, and immune-associated processes. The direction of methylation and expression changes varied among group contrasts. These regions and associated genes (Table 3) were selected based on an interactive analysis of overlapping genes between DEGs and DMRs, further reinforcing their regulatory relevance. For instance, *GPAM* was hypomethylated in BB vs. AA, while *ARG2* was hypermethylated. In CC vs. AA, hypomethylation of *ITGAV* and hypermethylation of *IDH3A*. The HH vs. AA and HH vs. BB groups exhibited multiple genes affected by hypermethylation (*ACO2*, *SDHB*, *TALDO1*, *B4GALT5*) and hypomethylation (*E2F7*, *UNG*).

Functional interpretation of DEG–DMR interactions

GO enrichment analysis of hypermethylated and downregulated genes identified biological process categories across all pairwise comparisons (Fig. 7). In BB vs. AA, enriched terms included negative regulation of CD4-positive, alpha–beta T cell activation. In CC vs AA and HH vs AA comparisons, enriched categories included cellular respiration. CC vs. BB enriched terms included positive regulation of myoblast fusion. In HH vs BB and HH vs

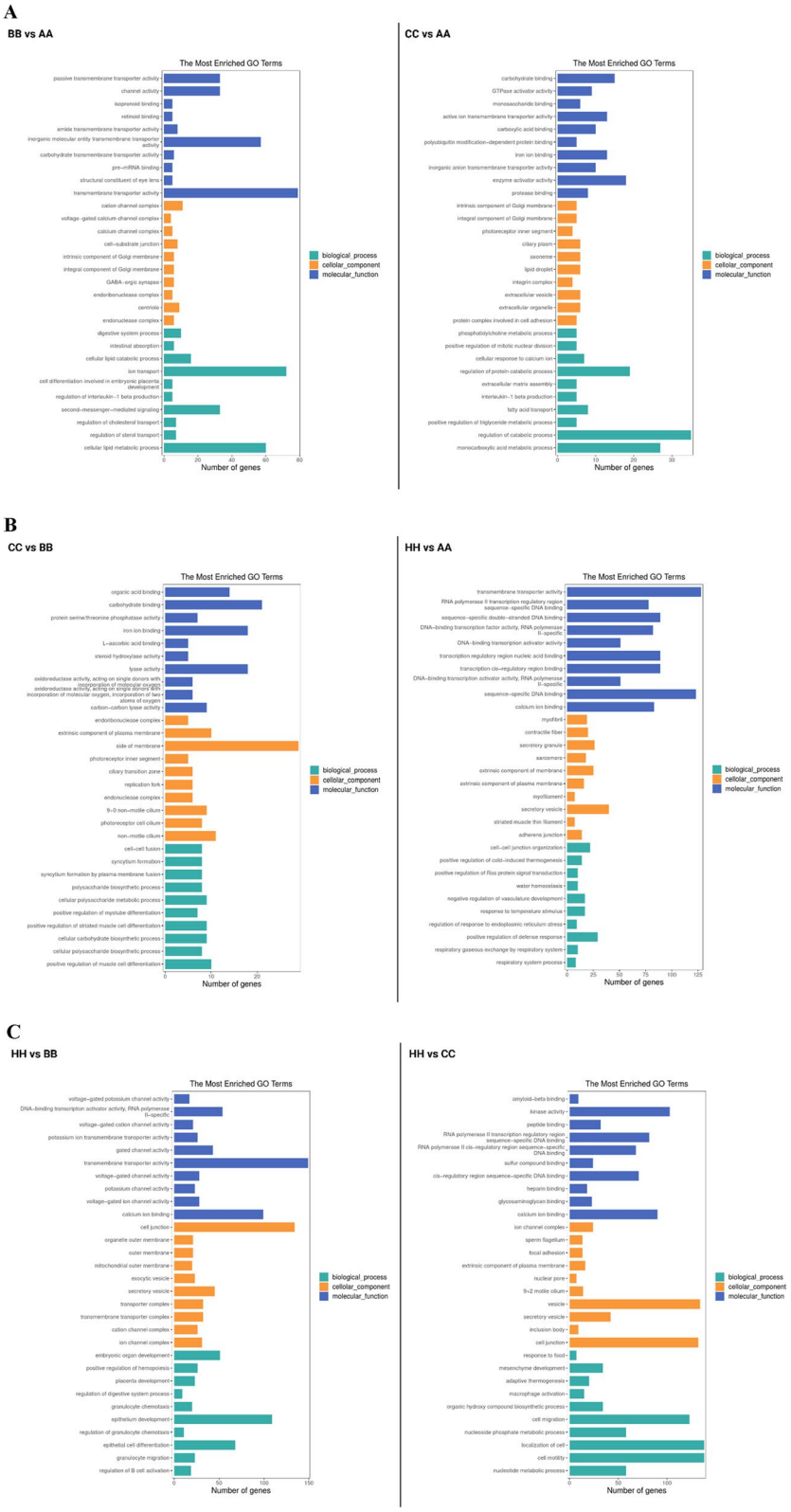

Fig. 5 GO terms in DMRs. **A** BB vs AA and CC vs AA. **B** CC vs BB and HH vs AA. **C** HH vs BB and HH vs CC

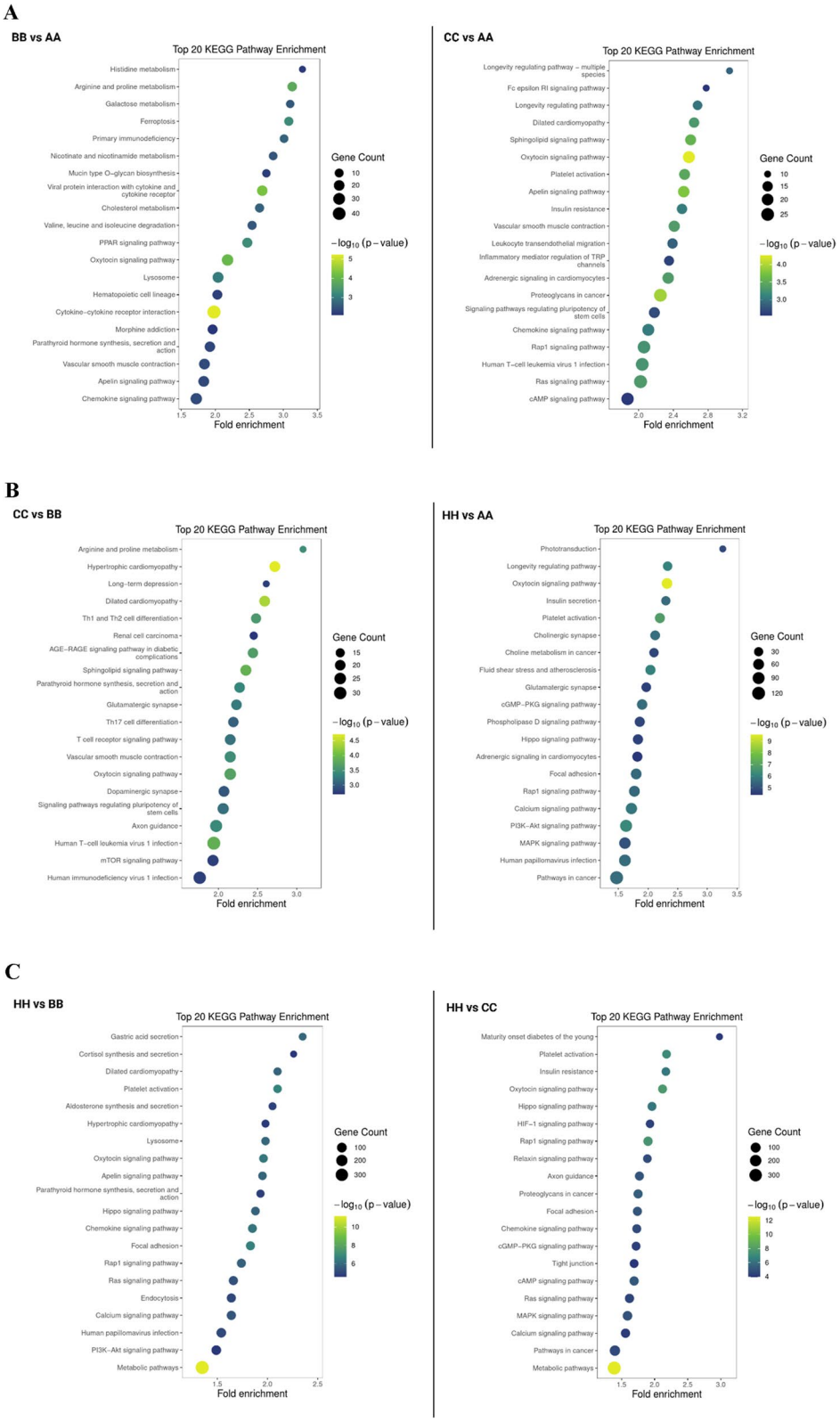

Fig. 6 KEGG pathway analysis of DMRs. **A** BB vs AA and CC vs AA. **B** CC vs BB and HH vs AA. **C** HH vs BB and HH vs CC

Table 2 Significantly expressed genes selected from RNA-Seq data

Genes	Description	Chr	P-adj	Log_2(FC)	Variation	Group
AICDA	Activation-Induced Cytidine Deaminase	chr5	3.13E-06	5.217764	↑	BB vs. AA
GPAM	Glycerol-3-phosphate acyltransferase, Mitochondrial	chr14	0.010487	1.491799	↑	BB vs. AA
ARG2	Arginase 2	chr7	0.000684	-2.06089	↓	BB vs. AA
AUH	AU RNA-binding Methylglutaconyl-CoA Hydratase	chr14	0.00137	-2.17896	↓	BB vs. AA
ITGAV	Integrin Subunit Alpha V	chr15	9.05E-10	3.596246	↑	CC vs. AA
IDH3A	Isocitrate Dehydrogenase (NAD (+)) 3 Catalytic Subunit Alpha	chr7	0.004534	-1.2382	↓	CC vs. AA
NDUFV1	NADH: ubiquinone Oxidoreductase Core Subunit V1	chr2	0.000566	-1.81382	↓	CC vs. AA
RAB21	RAB21, member RAS oncogene family	chr5	5.55E-10	3.004464	↑	CC vs. BB
TMEM199	transmembrane protein 199	chr12	0.000759	2.408357	↑	CC vs. BB
CD53	CD53 Molecule	chr4	0.026678	-7.31612	↓	CC vs. BB
CACNA2D1	Calcium Voltage-gated Channel Auxiliary Subunit Alpha2delta 1	chr9	0.000129	3.58063	↑	HH vs. AA
E2F7	E2F Transcription Factor 7	chr5	0.035581	2.806235	↑	HH vs. AA
NDUFS8	NADH: ubiquinone Oxidoreductase Core Subunit S8	chr2	0.013933	-1.2116	↓	HH vs. AA
UNG	Uracil DNA Glycosylase	chr14	0.00068	2.553054	↑	HH vs. BB
PNRC2	Proline Rich Nuclear Receptor Coactivator 2	chr6	0.01943	1.20761	↑	HH vs. BB
HLCS	Holocarboxylase Synthetase	chr13	0.009937	1.49628	↑	HH vs. BB
B4GALT5	beta-1,4-Galactosyltransferase 5	chr17	1.60E-05	-2.09688	↓	HH vs. BB
OSTC	Oligosaccharyltransferase complex non-catalytic Subunit	chr8	0.000964	-1.59399	↓	HH vs. BB
PLAU	Plasminogen Activator, Urokinase	chr14	6.21E-09	9.245213	↑	HH vs. CC
MRAP2	Melanocortin 2 Receptor Accessory Protein 2	chr1	0.017122	6.123966	↑	HH vs. CC
EXT1	Exostosin glycosyltransferase 1	chr4	4.88E-05	-2.13153	↓	HH vs. CC

(↓): Downregulation

(↑): Upregulation

CC contrasts, enriched processes included protein and macromolecular glycosylation.

GO enrichment analysis of hypomethylated and upregulated genes identified distinct biological process categories (Fig. 8). In BB vs. AA, enriched terms included viral RNA genome replication and protein palmitoylation. In CC vs. AA, enriched terms included substrate adhesion-dependent cell spreading. CC vs. BB exhibited significant enrichment in signaling processes, including calcineurin-mediated signaling and regulation of cellular pH. In HH vs. AA, enriched terms included cell differentiation related to embryonic placental development. In HH vs. BB, enriched terms included base-excision repair. In HH vs. CC, enriched terms included negative regulation of homeostasis and blood coagulation.

KEGG pathway analysis of overlapping genes identified enrichment in metabolic and regulatory pathways (Fig. 9). In HH vs BB (Fig. 9A), hypomethylated and upregulated genes were enriched in biotin metabolism. Hypermethylated and downregulated genes in HH vs AA, HH vs BB, and HH vs CC (Fig. 9B) were enriched in pathways including base excision repair, citrate cycle (TCA cycle), mucin-type glycan biosynthesis, and fatty acid elongation.

Discussion

The primary objective of this study was to explore the molecular effects of vitrification on porcine parthenogenetic blastocysts, with a particular focus on transcriptional and epigenetic changes and their impact on developmental competence. We comprehensively analyze how vitrification affects gene expression and DNA methylation patterns using advanced scRNA-seq and scWGBS. Our findings reveal that vitrification induces significant disruptions in key biological pathways, including energy metabolism, genomic stability, and cellular function. These changes reflect stress-induced impairments in hypermethylated and downregulated genes, as well as adaptive molecular responses in hypomethylated and upregulated genes. Moreover, this study demonstrates the advantages of LHe vitrification over LN vitrification in preserving these critical pathways, offering a promising approach to enhance blastocyst viability and developmental potential. However, it is crucial to recognize that blastocysts activated parthenogenetically exhibit differences in genomic DNA methylation compared to biparental embryos, which may influence their response to stress induced by vitrification. This factor could limit the broader applicability of our findings, as the dynamics of methylation and stress responses may differ significantly between parthenogenetic and fertilized embryos.

Our findings indicate that vitrification using liquid helium (LHe) offers both functional and molecular advantages over traditional liquid nitrogen (LN) methods. As presented in Table 1, the LHe group achieved the highest post-thaw survival rate, significantly surpassing both the modified liquid nitrogen (CC) and conventional

Table 3 Differentially Methylated Regions (DMRs) and associated genes selected from DNA methylation sequencing analysis

Genes	DMR	Q-value	Variation	Groups
GPAM	chr14: 122579148—122581148	0.02296	Hypomethylated	BB vs. AA
ARG2	chr7: 91341988—91343988	0.00002084	Hypermethylated	BB vs. AA
ITGAV	chr15: 91602676—91604676	0.01995	Hypomethylated	CC vs. AA
IDH3A	chr7: 47778956—47780956	0.00593	Hypermethylated	CC vs. AA
CD53	chr4: 109335802—109337802	0.006494	Hypermethylated	CC vs. BB
RAB21	chr5: 35755494—35757494	2.79E-11	Hypomethylated	CC vs. BB
ACO2	chr5: 7071025—7073025	0.0227	Hypermethylated	HH vs. AA
E2F7	chr5: 104125731—104127731	0.03891	Hypomethylated	HH vs. AA
SDHB	chr6: 75679556—75679810	0.0329	Hypermethylated	HH vs. AA
TALDO1	chr2: 462998—463228	9.92E-6	Hypermethylated	HH vs. AA
ACSL6	chr2: 134279379—134279538	0.0312	Hypomethylated	HH vs. AA
UNG	chr14: 41757807—41759807	0.0007725	Hypomethylated	HH vs. BB
B4GALT5	chr17: 51334020—51336020	0.001424	Hypermethylated	HH vs. BB
HACD2	chr13: 136832300—136832556	0.0000154	Hypermethylated	HH vs. BB
ELOVL5	chr7: 46934781—46934979	0.000209	Hypermethylated	HH vs. CC
DPM3	chr4: 94659873—94661873	0.0001899	Hypermethylated	HH vs. CC
PLAU	chr14: 76627299—76629299	3.705E-7	Hypomethylated	HH vs. CC

liquid nitrogen (BB) groups. This outcome underscores the enhanced cryoprotective efficacy of LHe. At the molecular level, embryos vitrified with LHe exhibited less downregulation of critical metabolic genes, such as *ACO2* and *NDUFS8*, which are essential for mitochondrial function. Furthermore, LHe-vitrified blastocysts demonstrated increased activation of DNA repair genes (*UNG*) and upregulation of genes involved in cell adhesion and signaling (*PLAU*, *MRAP2*), indicating improved developmental competence following thawing. While these molecular results suggest superior preservation of blastocyst integrity with LHe, further studies are required to validate its practical benefits concerning implantation and pregnancy outcomes, particularly in contexts where embryo manipulation aims to produce viable offspring [27].

The scRNA-seq results revealed an average mapping rate of 83.70% to the reference genome (Sus scrofa 11.1), with an average GC content of 47.23% (Supplementary Table S1). This mapping efficiency aligns with studies on vitrified porcine oocytes [17] and exceeds the rates observed in in vitro fertilized (IVF) and somatic cell nuclear transfer (SCNT) blastocysts [28]. Variations in GC content may reflect differences in biological characteristics or gene enrichment. The RNA-seq quality metrics showed high Q20 and Q30 scores across all samples, which confirm the reliability of the differential gene expression analysis. Additionally, scRNA-seq revealed significant differential gene expression ($P < 0.05$) across treatment groups, suggesting that vitrification induces transcriptional alterations in porcine blastocysts. These changes include downregulation of genes involved in metabolism, DNA repair, and development, and upregulation of stress-responsive genes. This dual response suggests that vitrification can disrupt essential cellular pathways while triggering compensatory mechanisms to preserve viability. Such alterations may impair lineage specification, metabolic balance, and implantation potential, highlighting the need to optimize vitrification conditions to minimize molecular damage and support embryonic development. Moreover, LHe vitrification (HH) yielded distinct transcriptional profiles with more DEGs than LN vitrification (CC), suggesting that LHe may better preserve key molecular pathways required for blastocyst survival and developmental competence.

In terms of epigenetic analysis (Supplementary Table S2), scWGBS revealed an average mapping rate of 33.69% and a bisulfite conversion efficiency of 99.27%, consistent with previous studies on bovine blastocysts derived from non-vitrified or vitrified oocytes [29], but lower than the rates (86–89%) in porcine piglet peripheral blood mononuclear cells (PBMCs) [30]. The GC content of 26–35% aligns with typical methylation data, highlighting the challenges in mapping bisulfite-treated sequences, particularly in regions with high GC content. These challenges likely reflect the inherent complexity of mapping bisulfite-converted sequences, which is influenced by factors such as sequence quality, reference genome quality,

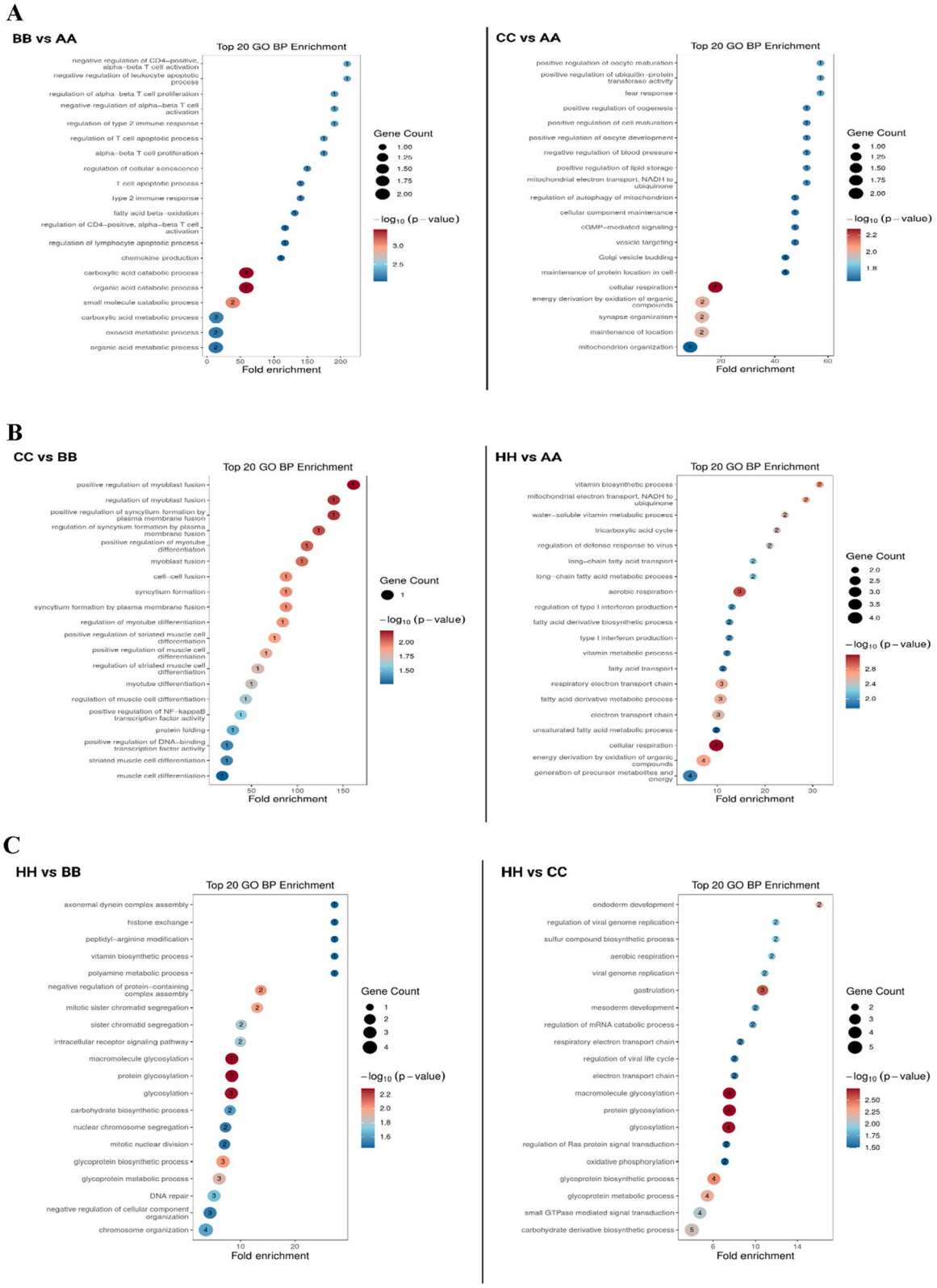

Fig. 7 GO analysis (Biological Processes) of hypermethylated and downregulated genes in group comparison. **A** BB vs AA and CC vs AA. **B** CC vs BB and HH vs AA. **C** HH vs BB and HH vs CC

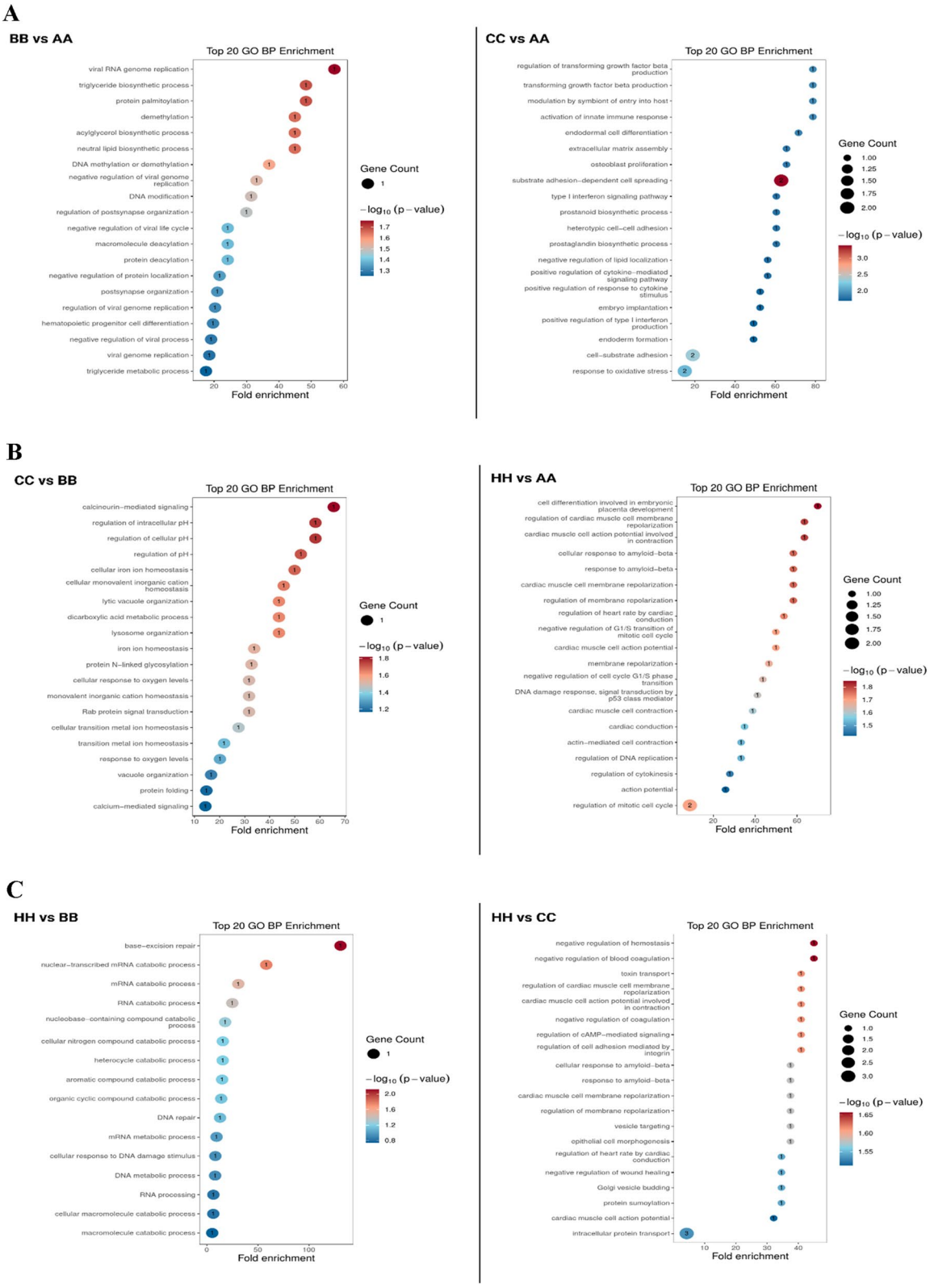

Fig. 8 GO analysis (Biological Processes) of hypomethylated and upregulated genes in group comparison. **A** BB vs AA and CC vs AA. **B** CC vs BB and HH vs AA. **C** HH vs BB and HH vs CC

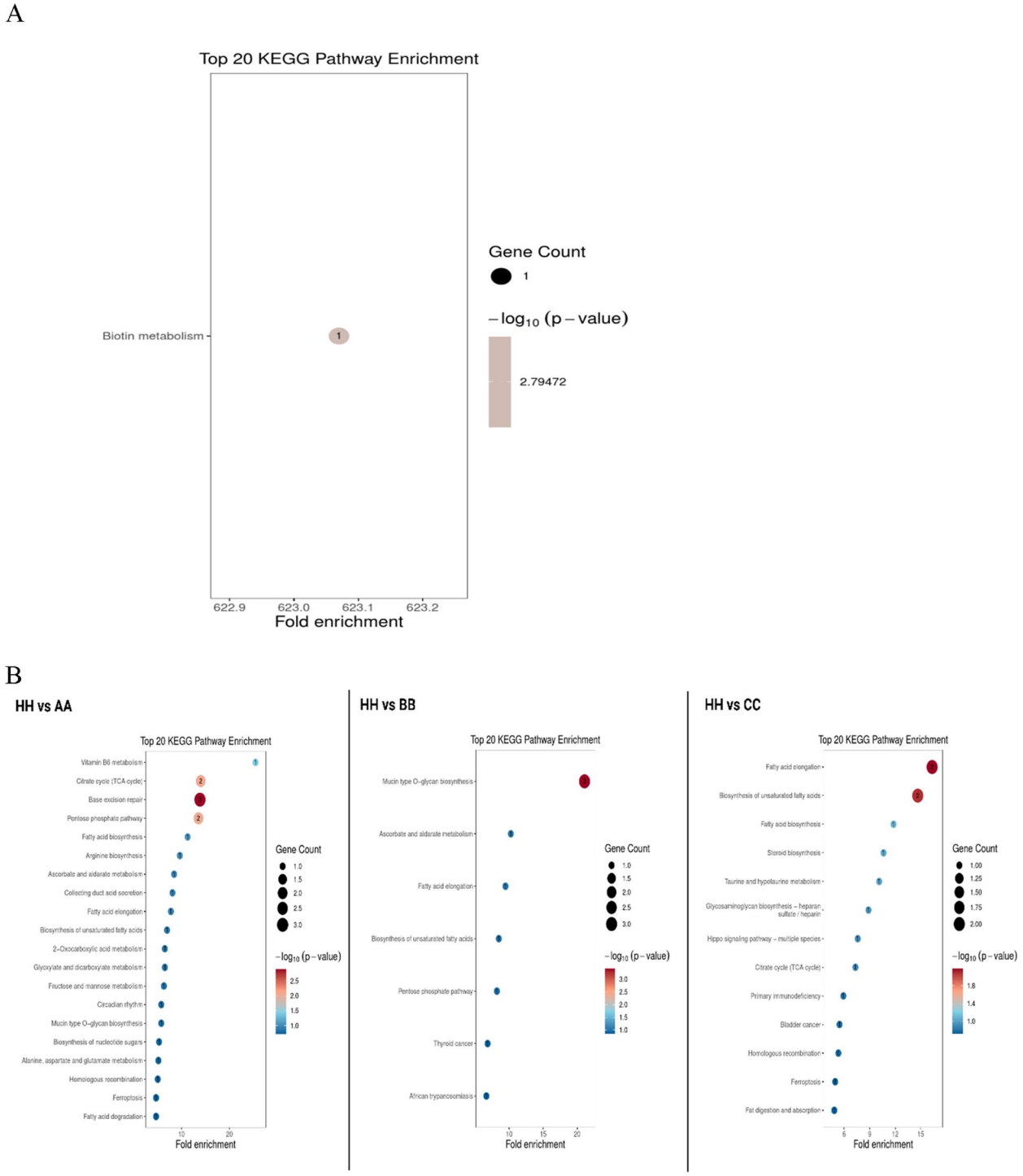

Fig. 9 KEGG Analysis. **A** KEGG analysis of hypomethylated and upregulated genes in HH vs. BB. **B** KEGG analysis of hypermethylated and downregulated genes in HH vs. AA, HH vs. BB, and HH vs. CC

genome complexity, sample quality, and sequencing depth. Additionally, scWGBS analysis further identified significant differential methylation, with both hyper-DMRs and hypo-DMRs exhibiting significant changes ($Q < 0.05$). We observed higher hypermethylation in HH vs. BB, which suggests gene silencing or epigenetic repression due to vitrification stress. In contrast, the higher hypomethylation in BB compared to AA suggests that vitrification (BB) may have caused a loss of DNA methylation in specific genomic regions, potentially leading to gene activation, altered cellular function, and an impact on blastocyst development and survival. Similarly,

HH vs. CC showed the highest background CG ratio, suggesting widespread involvement of cytosine-guanine sites in DNA methylation and epigenetic modifications induced by vitrification, which may influence gene regulation and blastocyst developmental competence. The observed differential methylation patterns suggest epigenetic reprogramming consistent with the dynamic, wave-like DNA methylation remodeling that characterizes early mammalian embryogenesis [31], a process known to be highly sensitive to perturbations in calcium-mediated activation signaling and chromatin remodeling in porcine embryos [32, 33]. Such perturbations may contribute to compensatory responses or developmental impairments in blastocysts. These results highlight the molecular effects of vitrification on epigenetic regulation, which may impact gene expression and embryonic development.

DNA methylation in gene promoters is a crucial epigenetic mechanism that regulates gene expression, often suppressing transcription by obstructing transcription factor binding and altering chromatin accessibility. Our study identified significant correlations between promoter methylation and changes in gene expression in vitrified blastocysts. For instance, hypermethylation of key metabolic genes, such as *IDH3A* and *ARG2*, was associated with their downregulation, thereby disrupting vital energy metabolism pathways and diminishing blastocyst viability. Conversely, hypomethylation of genes like *GPAM* and *ITGAV* correlated with their upregulation, indicating an adaptive response aimed at restoring metabolic balance and reducing oxidative stress following vitrification. These findings underscore the crucial role of promoter methylation in the embryonic response to vitrification stress, affecting developmental competence and survival.

Vitrification-induced hypermethylation and gene downregulation disrupt essential biological processes, significantly impairing the viability of porcine blastocysts (Tables 2 and 3). These disruptions were observed across various group comparisons and affected critical pathways, including energy metabolism, immune function, and protein glycosylation (Fig. 7). Excessive DNA methylation in key regulatory regions likely contributes to gene silencing, metabolic dysfunction, and impaired intercellular communication, collectively compromising post-thaw survival and implantation potential. The epigenetic silencing and transcriptional repression of these genes reduce mitochondrial efficiency, metabolic adaptability, and membrane-associated immune functions, all of which are crucial for blastocyst expansion and developmental competence. These findings demonstrate that vitrification induces a coordinated disruption of gene regulation, characterized by aberrant DNA methylation and transcriptional downregulation across interconnected biological pathways, ultimately compromising embryonic viability.

In the BB vs. AA comparison, downregulation of the *ARG2* and *AUH* genes was observed, enriched for processes related to organic acid and carboxylic acid catabolism. These metabolic pathways are critical for enhanced energy production, maintenance of cellular functions, and promotion of early embryonic development. The downregulation of *ARG2* likely impairs nitrogen metabolism and mitochondrial function, leading to reduced oxidative phosphorylation, metabolic stress, energy shortages, and increased susceptibility to oxidative damage, which may compromise blastocyst viability and developmental competence [34]. This observation aligns with the findings of Zhao et al. (2023) [35] who reported similar alterations in DEGs associated with metabolic pathways. Similarly, in CC vs. AA, downregulation of *IDH3A* and *NDUFV1* significantly impaired cellular respiration, mitochondrial electron transport, and energy derivation through the oxidation of organic compounds. Specifically, *IDH3A* plays a key role in energy production by catalyzing reactions in the tricarboxylic acid (TCA) cycle [36], while *NDUFV1* is involved in transferring electrons from NADH to ubiquinone within the mitochondrial electron transport chain [37]. The downregulation of these genes in BB vs. AA and CC vs. AA disrupts energy metabolism, potentially leading to energy deficits that reduce the blastocysts' ability to sustain growth and implantation. Furthermore, in the comparison of CC vs. BB, *CD53* was significantly downregulated, highlighting severe impairment of immune function. *CD53* is enriched in syncytium formation, plasma membrane fusion, and cell–cell communication, which are essential for immune signaling and embryonic development. This gene plays a critical role in supporting immune function through cell communication and membrane fusion, processes essential for the formation of syncytia and immune interactions [38]. The downregulation of *CD53* likely compromises the embryo's ability to respond to stress or infection, increasing its susceptibility to cellular damage and apoptosis. Reduced *CD53* expression could reduce the blastocyst's ability to establish maternal–fetal immune tolerance, increasing the risk of implantation failure and early pregnancy loss.

In addition to the previously discussed hypermethylated and downregulated genes, further analysis of the HH group revealed additional molecular changes reflecting blastocyst responses to cryopreservation stress (Fig. 7). In HH vs. AA, genes such as *ACO2* and *NDUFS8* were downregulated, affecting energy-related pathways, including cellular respiration, mitochondrial electron transport, energy derivation by oxidation of organic compounds, and the tricarboxylic acid (TCA) cycle. These pathways are crucial for ATP production

and biosynthesis, which are essential for supporting early embryonic development and maintaining cellular function [39]. Specifically, *ACO2* catalyzes the conversion of citrate to isocitrate in the TCA cycle, a key step in oxidative phosphorylation [40]. While NDUFS8 is a core component of complex I in the mitochondrial electron transport chain, facilitating ATP generation [41], further studies on pluripotent pig embryos confirm that *ACO2* downregulation coincides with the reduced expression of other electron transport complex genes. This suggests a metabolic shift from oxidative phosphorylation to glycolysis, which may reduce mitochondrial efficiency and impair blastocyst survival and implantation [42]. The downregulation of these genes in HH vs. AA suggests a stress-induced response that disrupts energy metabolism, potentially compromising blastocyst viability and developmental competence. In HH vs. BB and HH vs. CC comparisons, downregulation of *B4GALT5*, *OSTC*, *DPM3*, and *EXT1* was observed, indicating severe impairments in protein-related pathways, particularly glycosylation and glycoprotein biosynthesis. These processes are crucial for maintaining protein stability, regulating cell signaling, and facilitating early embryonic development [43]. Glycosylation plays a crucial role in regulating protein function, influencing cell interactions, and maintaining cellular communication. These processes closely interact with changes in DNA methylation, underscoring their significance in the complex molecular mechanisms of early embryonic development [44]. The downregulation of these genes likely disrupts post-translational modifications, leading to protein misfolding, defective signaling, and compromised cellular integrity. This disruption, in turn, may contribute to impaired embryonic development, reduced implantation potential, and increased susceptibility to stress.

Vitrification significantly alters transcriptional and epigenetic changes, triggering adaptive and adverse molecular responses. This study reveals hypomethylation and upregulation of key genes involved in energy metabolism (*GPAM*), DNA modification (*AICDA*), cell-substrate adhesion and oxidative stress response (*ITGAV*), cellular homeostasis (*TMEM199*, *RAB21*), DNA repair (*UNG*), and cell adhesion and signaling (*PLAU, MRAP2*) (Fig. 8). These hypomethylated and upregulated genes highlight critical biological processes essential for maintaining blastocyst viability, supporting recovery post-vitrification, and enhancing implantation potential. However, excessive upregulation of *GPAM*, *ITGAV*, *E2F7*, and *PLAU* due to vitrification may lead to metabolic exhaustion, oxidative stress accumulation, lipotoxicity, mitochondrial dysfunction, DNA damage, and disrupted cell signaling, collectively increasing the risk of cellular apoptosis, developmental arrest, and reduced embryo survival.

In the BB vs. AA comparison, upregulation of *GPAM* and *AICDA* was observed, highlighting their importance in energy storage and maintaining DNA integrity during cryopreservation. *GPAM* contributes to triglyceride biosynthesis, supporting energy metabolism [45] by maintaining energy reserves essential for implantation and early embryonic development [46]. Similarly, *AICDA* modulates DNA methylation and modification, regulating cell differentiation and genomic stability, which are essential for blastocyst development [47]. This aligns with Deshmukh et al. (2011) [48], who demonstrated that DNA methylation facilitates somatic genome reprogramming, a crucial process for proper embryonic development. However, excessive upregulation of *GPAM* and *AICDA* may result in metabolic imbalances, aberrant DNA modifications, and impaired differentiation, potentially compromising blastocyst viability and developmental competence. In the comparison between CC and AA, *ITGAV* was upregulated, highlighting its pivotal role in facilitating cell-substrate adhesion and the oxidative stress response, which is critical for blastocyst implantation and survival under stress induced by vitrification. *ITGAV*, a subunit of integrin receptors that mediate cell adhesion to the extracellular matrix, is crucial for implantation and early embryonic development [49]. By facilitating trophoblast attachment to the uterine lining, *ITGAV* enhances implantation efficiency and embryonic stability [50]. Its significant upregulation in the luminal epithelium of the porcine endometrium on Day 14 further underscores its role in implantation [51]. Additionally, *ITGAV* was enriched in oxidative stress response pathways that neutralize reactive oxygen species (ROS) and maintain cellular homeostasis in developing blastocysts [52]. However, excessive oxidative stress can trigger endoplasmic reticulum stress and apoptosis, impairing protein synthesis and mitochondrial function and compromising embryonic viability [53–55]. Notably, this pathway has been identified in vitrified, in vitro-cultured, and controlled porcine blastocysts [16]. Consistently, Zhang et al. (2020) [56] reported that vitrification alters gene expression associated with oxidative stress response, reinforcing the dual role of *ITGAV* in supporting and potentially compromising embryonic development under stress conditions. Furthermore, the upregulation of *TMEM199* and *RAB21* was identified in the CC compared to the BB, substantiating their importance in maintaining cellular homeostasis and facilitating adaptive responses, which are crucial for the survival of vitrified porcine blastocysts. *TMEM199*-enriched cellular pH regulation and iron homeostasis pathways contribute to ion transport, enzymatic activity, and cellular integrity [57, 58], thereby facilitating resilience under cryogenic conditions. Similarly, *RAB21*, which is involved in intracellular trafficking and signal transduction, regulates the

transport of receptors and proteins essential for cellular responses to environmental stress [59]. By facilitating efficient intracellular vesicular transport, *RAB21* ensures proper protein localization and communication between cellular compartments, which is crucial for stress resilience and maintaining cellular integrity in vitrified blastocysts [60]. The upregulation of these genes underscores their crucial roles in maintaining cellular stability, mitigating stress induced by vitrification, and promoting blastocyst survival and developmental potential.

In the HH vs. AA comparison, upregulation of *E2F7* was observed, highlighting its critical role in cell differentiation during embryonic placenta development, which is essential for supporting blastocyst growth and implantation. Cell differentiation regulates the segregation of the inner cell mass and trophectoderm, which is critical in early placental development [61]. Similarly, *E2F7* may enhance the adaptive response of HH blastocysts by preserving genome integrity through the regulation of the mitotic cell cycle and DNA repair mechanisms [62], thereby its upregulation may support the recovery of blastocysts post-vitrification and their implantation potential. However, excessive *E2F7* expression has been linked to increased DNA damage, which can disrupt cell cycle progression and elevate the risk of apoptosis, thereby compromising blastocyst viability [63]. Similarly, *CACNA2D1* was enriched in pathways related to calcium ion transport, reflecting its essential role in maintaining cellular communication, ion homeostasis, and stress adaptation mechanisms. *CACNA2D1*, a calcium channel subunit, modulates intracellular calcium signaling and is essential for metabolic activity, trophoblast invasion, and successful implantation [64]. The upregulation of *E2F7* and *CACNA2D1* suggests a coordinated molecular response to vitrification-induced stress, balancing placental development and ion regulation to support blastocyst survival. However, excessive activation of these pathways may induce metabolic imbalance, emphasizing the need for tightly regulated expression. In the HH vs. BB comparison, significant upregulation of the *UNG* gene was observed, which is associated with the base excision repair (BER) pathway and is responsible for maintaining genomic stability and repairing oxidative DNA damage induced by vitrification [65]. Vitrification induces oxidative DNA damage, and the upregulation of *UNG* in HH blastocysts suggests an enhanced repair capacity, promoting better recovery and developmental competence compared to BB blastocysts. Similarly, *PNRC2* was upregulated, which regulates RNA catabolism and degradation, indicating its role in preserving transcriptomic integrity and stress adaptation by maintaining proper mRNA processing [66]. The upregulation of *UNG* and *PNRC2* underscores the importance of coordinated DNA and RNA repair mechanisms in enhancing the resilience and developmental potential of vitrified blastocysts. Furthermore, in the comparison between HH and CC, PLAU and MRAP2 were upregulated, highlighting their roles in cell adhesion and cAMP-mediated signaling. *PLAU* encodes urokinase-type plasminogen activator (uPA), which binds to its receptor, uPAR, on the cell surface to activate signaling cascades that promote migration, adhesion, survival, and proliferation, all of which are critical for successful blastocyst implantation [67]. However, precise regulation of uPA activity is essential in blastocyst development; excessive or insufficient activity could disrupt normal cell adhesion dynamics, potentially impairing implantation and subsequent development [68]. Similarly, *MRAP2* modulates cAMP signaling, enhancing oocyte developmental competence and blastocyst quality in porcine IVF [69]. The upregulation of *PLAU* and *MRAP2* suggests a coordinated mechanism that promotes implantation and developmental competence, with regulated *PLAU* expression being crucial for maintaining adhesion dynamics in early embryogenesis.

Our findings revealed notable transcriptional and epigenetic effects associated with vitrification using LN and LHe, as evidenced by differences in GO enrichment analyses. Blastocysts vitrified with LN (BB vs. AA) demonstrated significant enrichment in GO terms related to energy metabolism, RNA binding, and mitochondrial functions, indicating disruptions in critical areas essential for embryonic development. In contrast, blastocysts vitrified with LHe (HH vs. AA) showed enrichment in terms associated with amide biosynthesis, oxidoreductase activity, and membrane proteins, suggesting potential effects on protein metabolism and oxidative stress responses. DNA methylation analyses revealed hypermethylation of genes involved in cellular respiration in the LHe group, while the LN group exhibited hypomethylation in metabolism-related genes. These findings underscore the distinct molecular effects of LN versus LHe vitrification, highlighting the superior preservation of crucial biological pathways and developmental potential offered by LHe.

KEGG pathway analysis showed that the hypermethylation and downregulation of key genes disrupted essential metabolic and regulatory pathways (Fig. 9B). In the HH vs. AA, HH vs. BB, and HH vs. CC comparisons, the downregulation of *SDHB*, *TALDO1*, *ACSL6*, *ELOVL5*, and *HACD2* impaired critical pathways, including the Citrate Cycle (TCA cycle), Pentose Phosphate Pathway (PPP), Homologous Recombination (HR), and Fatty Acid Biosynthesis. These pathways are fundamental for energy production, DNA repair, lipid metabolism, and cell membrane formation, and their disruption compromises blastocyst survival and development [70]. The PPP generates key metabolites for reductive biosynthesis, nucleotide synthesis, and oxidative stress regulation

[71]. Its enrichment is consistent with Zhai et al. (2022) [72], who reported that 21.4% of downregulated genes in 4-cell porcine SCNT embryos are enriched for similar pathways. Similarly, the HR pathway is essential for repairing DNA double-strand breaks and maintaining genomic stability during embryonic development [73]. Additionally, fatty acid biosynthesis is crucial for producing lipids that maintain membrane integrity, provide energy storage, and facilitate signaling processes essential for blastocyst survival and development [74]. Researchers have linked dysregulation of fatty acid metabolism to subfertility and impaired embryo development, underscoring the importance of understanding these pathways to enhance livestock reproductive health [75]. Specifically, the downregulation of *SDHB* and *TALDO1* may reduce mitochondrial efficiency and ATP production, thereby impairing mitochondrial metabolic coordination during early embryogenesis [76], while the disruption of *ACSL6* and *ELOVL5* compromises lipid metabolism, impairing cellular function and blastocyst development. Conversely, hypomethylated and upregulated genes were significantly enriched in metabolic and regulatory pathways supporting porcine blastocyst development after vitrification (Fig. 7A). Notably, the biotin metabolism pathway was significantly enriched in HH vs. BB, with the *HLCS* gene playing a central role in energy generation, biosynthesis, and gene regulation, which are essential for cellular integrity [77]. *HLCS* upregulation enhances biotin-dependent enzymes that drive energy production, biosynthesis, and gene regulation, supporting cellular integrity and blastocyst development [78]. *HLCS* upregulation and biotin metabolism may underlie the enhanced recovery and developmental competence of helium-vitrified blastocysts, emphasizing helium's role in preserving key metabolic pathways during cryopreservation.

Conclusion

This study demonstrates that vitrification alters transcriptional and epigenetic regulation in porcine parthenogenetically activated blastocysts, affecting energy metabolism, genomic stability, cellular homeostasis, and immune function. Key gene disruptions, including the downregulation of *ARG2*, *AUH*, *IDH3A*, *NDUFV1*, *CD53*, *B4GALT5*, *OSTC*, *DPM3*, and *EXT1*, impair mitochondrial function, protein glycosylation, and immune responses, leading to metabolic stress and reduced implantation potential. Conversely, the upregulation of *GPAM*, *ITGAV*, *PLAU*, *MRAP2*, *TMEM199*, and *RAB21* suggests compensatory mechanisms, though excessive activation may cause cellular stress. Notably, our study conclusively demonstrates that blastocysts vitrified using LHe exhibit significantly better developmental potential compared to those vitrified with LN, as evidenced by blastocyst survival assessment with the LHe group exhibiting the highest post-thaw survival rate, superior molecular integrity, reduced transcriptomic and epigenetic alterations, and improved maintenance of essential pathways related to energy metabolism, genomic stability, and cellular homeostasis. LHe showed better preservation of molecular integrity compared to LN vitrification, highlighting its potential to improve post-thaw blastocyst viability. Future studies should focus on refining vitrification protocols to minimize molecular stress and enhance embryo survival in assisted reproductive technologies.

Future investigations should extend these findings by evaluating the long-term developmental competence of vitrified embryos, including implantation efficiency, pregnancy outcomes, and offspring health. Integration of additional multi-omics approaches, such as chromatin accessibility profiling and single-cell proteomics, would further clarify the regulatory networks underlying cryo-induced molecular alterations. Moreover, mechanistic studies examining the fidelity of epigenetic reprogramming during post-warming development will be essential to determine whether ultra-rapid cooling strategies, such as LHe vitrification, confer sustained developmental advantages. Collectively, these efforts will help refine cryopreservation protocols for reproductive biotechnology and improve the safety and reliability of embryo preservation in both agricultural and biomedical contexts.

Abbreviations

ARG2	Arginase 2
AUH	AU RNA-binding Methylglutaconyl-CoA Hydratase
IDH3A	Isocitrate Dehydrogenase (NAD (+)) 3 Catalytic Subunit Alpha
NDUFV1	NADH: ubiquinone Oxidoreductase Core Subunit V1
CD53	CD53 Molecule
B4GALT5	Beta-1,4-Galactosyltransferase 5
OSTC	Oligosaccharyltransferase complex non-catalytic Subunit
DPM3	Dolichyl-Phosphate Mannosyltransferase Subunit 3, Regulatory
EXT1	Exostosin glycosyltransferase 1
GPAM	Glycerol-3-phosphate acyltransferase, Mitochondrial
AICDA	Activation-Induced Cytidine Deaminase
ITGAV	Integrin Subunit Alpha V
PLAU	Plasminogen Activator, Urokinase
MRAP2	Melanocortin 2 Receptor Accessory Protein 2
RAB21	RAB21, member RAS oncogene family
TMEM199	Transmembrane protein 199
CACNA2D1	Calcium Voltage-gated Channel Auxiliary Subunit Alpha2delta 1
E2F7	E2F Transcription Factor 7
ACOS2	Aconitase 2
NDUFS8	NADH: ubiquinone Oxidoreductase Core Subunit S8
UNG	Uracil DNA Glycosylase
PNRC2	Proline Rich Nuclear Receptor Coactivator 2
HLCS	Holocarboxylase Synthetase
SDHB	Succinate Dehydrogenase Complex Iron Sulfur Subunit B
TALDO1	Transaldolase 1
ACSL6	Acyl-CoA Synthetase Long Chain Family Member 6
HACD2	3-Hydroxyacyl-CoA Dehydratase 2
EVOVL5	Elongation of Very Long Chain Fatty Acids Protein 5

Supplementary Information

The online version contains supplementary material available at https://doi.org/10.1186/s12864-026-12752-5.

Supplementary Material 1.

Supplementary Material 2.

Supplementary Material 3.

Supplementary Material 4.

Authors' contributions

All the authors contributed to the writing of this review paper. All authors have read and approved the final manuscript. Writing-original draft preparation: J.O.A, B.Y; Conceptualization: J.O.A, B.Y, J.D, X.F; Methodology: B.Y, J.D, X.F, M.S, and H.A.K; Resources: J.O.A, B.Y, J.D, X.F; Writing-review and editing: J.O.A, B.Y, M.S, H.A.K, P.W, H.P, and X.Z; Supervision: P.W, H.P, and X.Z; Project administration: H.P and X.Z; Funding acquisition: H.P and X.Z. All authors have read and agreed to the published version of the manuscript.

Funding

This work was supported by the Strategic Cooperation Funding Project between Chongqing Municipal Government and Chinese Academy of Agricultural Sciences (23310), Specially Appointed Expert Program of Tianchi Talent Program in Xinjiang Province (Xueming Zhao), the National Natural Science Foundation of China (32161143032), the earmarked fund for CARS (CARS36-16), the National Germplasm Center of Domestic Animal Resources and the Agricultural Science and Technology Innovation Program (ASTIP-2016-IAS-06).

Data availability

All data generated or analyzed during this study are included in this published article, its supplementary information files, and publicly available repositories. The raw sequence data for scRNA-seq and scWGBS have been deposited in the NCBI Gene Expression Omnibus (GEO) (https://ncbi.nlm.nih.gov/geo/) under accession numbers GSE305944 and GSE305947, respectively.

Declarations

Ethics approval and consent to participate

Not applicable.

Consent for publication

Not applicable.

Competing interests

The authors declare no competing interests.

Author details

[1]Institute of Animal Sciences (IAS), Chinese Academy of Agricultural Sciences (CAAS), No.2 Yuanmingyuan Western Road, Haidian District, Beijing 100193, People's Republic of China
[2]State Key Laboratory of Sheep Genetic Improvement and Healthy Breeding, Institute of Animal Husbandry and Veterinary Sciences, Xinjiang Academy of Agricultural and Reclamation Sciences, Shihezi, China
[3]Chongqing Academy of Animal Sciences, Chongqing 402460, China

Received: 6 August 2025 / Accepted: 11 March 2026
Published online: 02 April 2026

References

1. Casciani V, Monseur B, Cimadomo D, Alvero R, Rienzi L. Oocyte and embryo cryopreservation in assisted reproductive technology: past achievements and current challenges. Fertil Steril. 2023;120:506–20. https://doi.org/10.1016/j.fertnstert.2023.06.005. (Elsevier Inc).
2. Morado S, Aparicio A, Pinchetti D, Arraztoa CC, Alvarez G, Gutnisky C, et al. Variations in metabolic parameters of in vitro matured porcine oocytes after vitrification-warming. Open Vet J. 2023;13:1416–24. https://doi.org/10.5455/OVJ.2023.V13.I11.4. (Faculty of Veterinary Medicine, University of Tripoli).
3. Xingzhu D, Qingrui Z, Keren C, Yuxi L, Yunpeng H, Shien Z, et al. Cryopreservation of porcine embryos: recent updates and progress. Biopreserv Biobank. 2021;19:210–8. https://doi.org/10.1089/bio.2020.0074.
4. Fahy GM, Wowk B. Principles of Ice-Free Cryopreservation by Vitrification. In: Wolkers Willem F. and Oldenhof H, editor. Cryopreservation and Freeze-Drying Protocols. New York, NY: Springer US; 2021. p. 27–97. https://doi.org/10.1007/978-1-0716-0783-1_2.
5. Taniguchi M, Ikeda A, Arikawa E, Wongsrikeao P, Agung B, Naoi H, et al. Effect of cryoprotectant composition on in vitro viability of in vitro fertilized and cloned bovine embryos following vitrification and in-straw dilution. J Reprod Dev. 2007;53(4):963.
6. Kamoshita M, Sugita H, Kageyama A, Kawata Y, Ito J, Kashiwazaki N. Recent advances of oocyte/embryo vitrification in mammals from rodents and large animals. Animal Science Journal. John Wiley and Sons Inc; 2024. https://doi.org/10.1111/asj.13931.
7. Nakano K, Matsunari H, Nakayama N, Ogawa B, Kurome M, Takahashi M, et al. Cloned porcine embryos can maintain developmental ability after cryopreservation at the morula stage. J Reprod Dev. 2011;57(2):312–6.
8. Yu XL, Xu YK, Wu H, Guo XF, Li XX, Han WX, et al. Successful vitrification of bovine immature oocyte using liquid helium instead of liquid nitrogen as cryogenic liquid. Theriogenology. 2016;85:1090–6. https://doi.org/10.1016/j.theriogenology.2015.11.020.
9. Wu H, Yu XL, Guo XF, Zhang F, Pei XZ, Li XX, et al. Effect of liquid helium vitrification on the ultrastructure and related gene expression of mature bovine oocytes after vitrifying at immature stage. Theriogenology. 2017;87:91–9. https://doi.org/10.1016/j.theriogenology.2016.08.010.
10 Dou M, Lu C, Liu J, Rao W. Liquid helium enhanced vitrification efficiency of human bone-derived mesenchymal stem cells and human embryonic stem cells. Bioengineering. 2021;8:162. https://doi.org/10.3390/bioengineering8110162. (MDPI).
11. Chen JY, Li XX, Xu YK, Wu H, Zheng JJ, Yu XL. Developmental competence and gene expression of immature oocytes following liquid helium vitrification in bovine. Cryobiology. 2014;69:428–33. https://doi.org/10.1016/j.cryobiol.2014.09.380.
12. Mateo-Otero Y, Yeste M, Damato A, Giaretta E. Cryopreservation and oxidative stress in porcine oocytes. Res. Vet. Sci. Elsevier B.V.; 2021. p. 20–6. https://doi.org/10.1016/j.rvsc.2020.12.024.
13. Lim J, Park C, Kim M, Kim H, Kim J, Lee DS. Advances in single-cell omics and multiomics for high-resolution molecular profiling. Exp. Mol. Med. Springer Nature; 2024. p. 515–26. https://doi.org/10.1038/s12276-024-01186-2.
14. Xu T, Liu C, Zhang M, Wang X, Yan Y, Liu Q, et al. Vitrification of pronuclear zygotes perturbs porcine zygotic genome activation. Animals. 2022;12:610. https://doi.org/10.3390/ani12050610. (MDPI).
15. Sinclair KD. Developmental epigenetics: Understanding genetic and sexually dimorphic responses to parental diet and outcomes following assisted reproduction. J Dairy Sci. 2024; https://doi.org/10.3168/jds.2024-25811.
16 Almiñana C, Dubuisson F, Bauersachs S, Royer E, Mermillod P, Blesbois E, et al. Unveiling how vitrification affects the porcine blastocyst: clues from a transcriptomic study. J Anim Sci Biotechnol. 2022;13:46. https://doi.org/10.1186/s40104-021-00672-1. (BioMed Central Ltd).
17. Jia B, Xiang D, Yang H, Liang J, Lv C, Yang Q, et al. Transcriptome analysis of porcine embryos derived from oocytes vitrified at the germinal vesicle stage. Theriogenology. 2024;218:99–110. https://doi.org/10.1016/j.theriogenology.2024.01.032.
18. Wiesak T, Goryszewska-Szczurek E. Effect of vitrification on the expression of genes in porcine blastocysts derived from in vitro matured oocytes. Syst Biol Reprod Med. 2022;68:239–46. https://doi.org/10.1080/19396368.2022.2072788. (Taylor and Francis Ltd).
19. Cuello C, Martinez CA, Cambra JM, Parrilla I, Rodriguez-Martinez H, Gil MA, et al. Effects of vitrification on the blastocyst gene expression profile in a porcine model. Int J Mol Sci. 2021;22:1–14. https://doi.org/10.3390/ijms22031222. (MDPI AG).
20. Silvestre MA, Alfonso J, García-Mengual E, Salvador I, Duque CC, Molina I. Effect of recombinant human follicle-stimulating hormone and luteinizing hormone on in vitro maturation of porcine oocytes evaluated by the subsequent in vitro development of embryos obtained by in vitro fertilization, intracytoplasmic sperm injection, or parthenogenetic activation. J Anim Sci. 2007;85:1156–60. https://doi.org/10.2527/jas2006-645.
21. Currin L, Glanzner WG, Gutierrez K, de Macedo MP, Guay V, Baldassarre H, et al. Optimizing swine in vitro embryo production with growth factor and

antioxidant supplementation during oocyte maturation. Theriogenology. 2022;194:133–43. https://doi.org/10.1016/j.theriogenology.2022.10.005. (Elsevier Inc).
22. Li L, Han Q, Chen Y, Zhang M, Wang L, An X, et al. β-nicotinamide mononucleotide rescues the quality of aged oocyte and improves subsequent embryo development in pigs. PLoS One. Public Library of Science; 2023;18. https://doi.org/10.1371/journal.pone.0291640.
23. Gonzalez-Plaza A, Cambra JM, Garcia-Canovas M, Parrilla I, Gil MA, Martinez EA, et al. Cryotop vitrification of large batches of pig embryos simultaneously provides excellent postwarming survival rates and minimal interference with gene expression. Theriogenology. 2023;206:1–10. https://doi.org/10.1016/j.theriogenology.2023.04.011.
24. Wu GQ, Quan GB, Shao QY, Lv CR, Jiang YT, Zhao ZY, et al. Cryotop vitrification of porcine parthenogenetic embryos at the early developmental stages. Theriogenology. 2016;85:434–40. https://doi.org/10.1016/j.theriogenology.2015.09.015.
25. Singh M, Al-Eryani G, Carswell S, Ferguson JM, Blackburn J, Barton K, et al. High-throughput targeted long-read single cell sequencing reveals the clonal and transcriptional landscape of lymphocytes. Nat Commun. Nature Publishing Group; 2019;10. https://doi.org/10.1038/s41467-019-11049-4.
26. Smallwood SA, Lee HJ, Angermueller C, Krueger F, Saadeh H, Peat J, et al. Single-cell genome-wide bisulfite sequencing for assessing epigenetic heterogeneity. Nat Methods. 2014;11:817–20. https://doi.org/10.1038/nmeth.3035.
27. Gong G, Dai Y, Fan B, Zhu H, Zhu S, Wang H, et al. Birth of calves expressing the enhanced green fluorescent protein after transfer of fresh or vitrified/thawed blastocysts produced by somatic cell nuclear transfer. Mol Reprod Dev. 2004;69:278–88. https://doi.org/10.1002/mrd.20130.
28. Xu WH, Li ZC, Ouyang ZP, Yu B, Shi JS, Liu DW, et al. RNA-Seq transcriptome analysis of porcine cloned and in vitro fertilized blastocysts. J Integr Agric. 2015;14:926–38. https://doi.org/10.1016/S2095-3119(14)60866-2. (Editorial Department of Scientia Agricultura Sinica).
29. Zhao YH, Wang JJ, Zhang PP, Hao HS, Pang YW, Wang HY, et al. Oocyte IVM or vitrification significantly impairs DNA methylation patterns in blastocysts as analysed by single-cell whole-genome methylation sequencing. Reprod Fertil Dev. 2020;32:676–89. https://doi.org/10.1071/RD19234. (CSIRO).
30. Corbett RJ, Luttman AM, Herrera-Uribe J, Liu H, Raney NE, Grabowski JM, et al. Assessment of DNA methylation in porcine immune cells reveals novel regulatory elements associated with cell-specific gene expression and immune capacity traits. BMC Genomics. BioMed Central Ltd; 2022;23. https://doi.org/10.1186/s12864-022-08773-5.
31. Samiec M, Trzcińska M. From genome to epigenome: who is a predominant player in the molecular hallmarks determining epigenetic mechanisms underlying ontogenesis? Reprod Biol. 2024. https://doi.org/10.1016/j.repbio.2024.100965. (Elsevier B.V).
32. Samiec M, Skrzyszowska M, Lipiński D. Pseudophysiological transcomplementary activation of reconstructed oocytes as a highly efficient method used for producing nuclear-transferred pig embryos originating from transgenic foetal fibroblast cells. Pol J Vet Sci. 2012;15:509–16. https://doi.org/10.2478/v10181-012-0078-3.
33. Tian JH, Wu ZH, Liu L, Cai Y, Zeng SM, Zhu SE, et al. Effects of oocyte activation and sperm preparation on the development of porcine embryos derived from in vitro-matured oocytes and intracytoplasmic sperm injection. Theriogenology. 2006;66:439–48. https://doi.org/10.1016/j.theriogenology.2005.10.026.
34. Dowling JK, Afzal R, Gearing LJ, Cervantes-Silva MP, Annett S, Davis GM, et al. Mitochondrial arginase-2 is essential for IL-10 metabolic reprogramming of inflammatory macrophages. Nat Commun. Nature Research; 2021;12. https://doi.org/10.1038/s41467-021-21617-2.
35. Zhao J, Wang W, Zhang L, Zhang J, Sturmey R, Zhang J. Dynamic metabolism during early mammalian embryogenesis. Development (Cambridge). Company of Biologists Ltd; 2023. https://doi.org/10.1242/dev.202148.
36. May JL, Kouri FM, Hurley LA, Liu J, Tommasini-Ghelfi S, Ji Y, et al. IDH3α regulates one-carbon metabolism in glioblastoma. Sci. Adv. 2019. https://www.science.org.
37. Srivastava A, Srivastava KR, Hebbar M, Galada C, Kadavigrere R, Su F, et al. Genetic diversity of NDUFV1-dependent mitochondrial complex I deficiency. Eur J Hum Genet. 2018;26:1582–7. https://doi.org/10.1038/s41431-018-0209-0. (Nature Publishing Group).
38. Dunlock VME, Arp AB, Singh SP, Charrin S, Nguyen V, Jansen E, et al. Tetraspanin CD53 controls T cell immunity through regulation of CD45RO stability, mobility, and function. Cell Rep. Elsevier B.V.; 2022;39. https://doi.org/10.1016/j.celrep.2022.111006.
39. Arnold PK, Finley LWS. Regulation and function of the mammalian tricarboxylic acid cycle. J Biol Chem. 2023. https://doi.org/10.1016/j.jbc.2022.102838. (American Society for Biochemistry and Molecular Biology Inc.).
40. Chen Y, Cai GH, Xia B, Wang X, Zhang CC, Xie BC, et al. Mitochondrial aconitase controls adipogenesis through mediation of cellular ATP production. FASEB J. 2020;34:6688–702. https://doi.org/10.1096/fj.201903224RR. (John Wiley and Sons Inc.).
41. Wang S, Kang Y, Wang R, Deng J, Yu Y, Yu J, et al. Emerging roles of NDUFS8 located in mitochondrial complex I in different diseases. Molecules. 2022. https://doi.org/10.3390/molecules27248754. (MDPI).
42. Ramos-Ibeas P, Sang F, Zhu Q, Tang WWC, Withey S, Klisch D, et al. Pluripotency and X chromosome dynamics revealed in pig pre-gastrulating embryos by single cell analysis. Nat Commun. Nature Publishing Group; 2019;10. https://doi.org/10.1038/s41467-019-08387-8.
43. Scheper AF, Schofield J, Bohara R, Ritter T, Pandit A. Understanding glycosylation: regulation through the metabolic flux of precursor pathways. Biotechnol Adv. 2023. https://doi.org/10.1016/j.biotechadv.2023.108184. (Elsevier Inc.).
44. Wang J, Tian GG, Li X, Sun Y, Cheng L, Li Y, et al. Integrated glycosylation patterns of glycoproteins and DNA methylation landscapes in mammalian oogenesis and preimplantation embryo development. Front Cell Dev Biol. 2020. https://doi.org/10.3389/fcell.2020.00555. (Frontiers Media S.A.).
45. Mitka I, Ropka-Molik K, Tyra M. Functional analysis of genes involved in glycerolipids biosynthesis (GPAT1 and GPAT2) in pigs. Animals. 2019. https://doi.org/10.3390/ani9060308. (MDPI AG).
46. McLelland GL, Lopez-Osias M, Verzijl CRC, Ellenbroek BD, Oliveira RA, Boon NJ, et al. Identification of an alternative triglyceride biosynthesis pathway. Nature. 2023;621:171–8. https://doi.org/10.1038/s41586-023-06497-4. (Nature Research).
47. Greenberg MVC, Bourc'his D. The diverse roles of DNA methylation in mammalian development and disease. Nat. Rev. Mol. Cell Biol. Nature Publishing Group; 2019. p. 590–607. https://doi.org/10.1038/s41580-019-0159-6.
48. Deshmukh RS, Østrup O, Østrup E, Vejlsted M, Niemann H, Lucas-Hahn A, et al. DNA methylation in porcine preimplantation embryos developed in vivo and produced by in vitro fertilization, parthenogenetic activation and somatic cell nuclear transfer. Epigenetics. 2011;6:177–87. https://doi.org/10.4161/epi.6.2.13519. (Taylor and Francis Inc.).
49. Merino-Pérez A, Segura-Benítez M, Pellicer A, Cervelló I, Ferrero H. Unveiling the role of extracellular vesicles in reproductive success and uterine diseases - a systematic review. Reprod Biomed Online. 2025;51:104862. https://doi.org/10.1016/j.rbmo.2025.104862.
50. Tan B, Zhou C, Zang X, Zhao X, Xiao L, Zeng J, et al. Integrated Analysis of DNA Methylation and Gene Expression in Porcine Placental Development. Int J Mol Sci. Multidisciplinary Digital Publishing Institute (MDPI); 2023;24. https://doi.org/10.3390/ijms24065169.
51. Zeng S, Ulbrich SE, Bauersachs S. Spatial organization of endometrial gene expression at the onset of embryo attachment in pigs. BMC Genomics. BioMed Central; 2019;20. https://doi.org/10.1186/s12864-019-6264-2.
52. Hong Y, Boiti A, Vallone D, Foulkes NS. Reactive Oxygen Species Signaling and Oxidative Stress: Transcriptional Regulation and Evolution. Antioxidants. Multidisciplinary Digital Publishing Institute (MDPI); 2024. https://doi.org/10.3390/antiox13030312.
53. Marsico TV, Silva MV, Valente RS, Annes K, Rissi VB, Glanzner WG, et al. Unraveling the Consequences of Oxygen Imbalance on Early Embryo Development: Exploring Mitigation Strategies. Animals. Multidisciplinary Digital Publishing Institute (MDPI); 2023. https://doi.org/10.3390/ani13132171.
54. Samiec M, Wiater J, Wartalski K, Skrzyszowska M, Trzcińska M, Lipiński D, et al. The relative abundances of human leukocyte antigen-e, α-galactosidase a and α-gal antigenic determinants are biased by trichostatin a-dependent epigenetic transformation of triple-transgenic pig-derived dermal fibroblast cells. Int J Mol Sci. MDPI; 2022;23. https://doi.org/10.3390/ijms231810296.
55. Wartalski K, Wiater J, Maciak P, Pastuła A, Lis GJ, Samiec M, et al. Anabolic Steroids Activate the NF-κB Pathway in Porcine Ovarian Putative Stem Cells Independently of the ZIP-9 Receptor. Int J Mol Sci. Multidisciplinary Digital Publishing Institute (MDPI); 2024;25. https://doi.org/10.3390/ijms25052833.
56. Zhang L, Qi X, Ning W, Shentu L, Guo T, Zhang X, et al. Single-cell transcriptome profiling revealed that vitrification of somatic cloned porcine blastocysts causes substantial perturbations in gene expression. Front Genet. Frontiers Media S.A.; 2020;11. https://doi.org/10.3389/fgene.2020.00640.

57. Miles AL, Burr SP, Grice GL, Nathan JA. The vacuolar-ATPase complex and assembly factors, TMEM199 and CCDC115, control HIF1α prolyl hydroxylation by regulating cellular iron levels. Elife. 2017;6:e22693. https://doi.org/10.7554/eLife.22693. (eLife Sciences Publications, Ltd).
58. Doyen D, Poët M, Jarretou G, Pisani DF, Tauc M, Cougnon M, et al. Intracellular pH control by membrane transport in mammalian cells. insights into the selective advantages of functional redundancy. Front. Mol. Biosci. Frontiers Media S.A.; 2022. https://doi.org/10.3389/fmolb.2022.825028.
59. Bhuin T, Roy JK. Rab proteins: The key regulators of intracellular vesicle transport. Exp. Cell Res. Academic Press Inc.; 2014. p. 1–19. https://doi.org/10.1016/j.yexcr.2014.07.027.
60. Del Olmo T, Lacarriere-Keïta C, Normandin C, Jean D, Boisvert FM, Jean S. RAB21 interacts with TMED10 and modulates its localization and abundance. Biol Open. Company of Biologists Ltd; 2019;8. https://doi.org/10.1242/bio.045336.
61. Sawai K. Roles of cell differentiation factors in preimplantation development of domestic animals. J Reprod Dev. 2021;67:161–5.
62. Campos A, Clemente-Blanco A. Cell cycle and DNA repair regulation in the damage response: protein phosphatases take over the reins. Int J Mol Sci. 2020. https://doi.org/10.3390/ijms21020446. (MDPI AG).
63. Mitxelena J, Apraiz A, Vallejo-Rodríguez J, García-Santisteban I, Fullaondo A, Alvarez-Fernández M, et al. An E2F7-dependent transcriptional program modulates DNA damage repair and genomic stability. Nucleic Acids Res. 2018;46:4546–59. https://doi.org/10.1093/nar/gky218.
64. Yao X, Gao S, Yan N. Structural biology of voltage-gated calcium channels. Channels. Taylor and Francis Ltd.; 2023;18. https://doi.org/10.1080/19336950.2023.2290807.
65. Carter RJ, Parsons JL. Base excision repair, a pathway regulated by posttranslational modifications. Mol Cell Biol. 2016;36:1426–37. https://doi.org/10.1128/mcb.00030-16. (Informa UK Limited).
66. Cho H, Han S, Choe J, Park SG, Choi SS, Kim YK. SMG5-PNRC2 is functionally dominant compared with SMG5-SMG7 in mammalian nonsense-mediated mRNA decay. Nucleic Acids Res. 2013;41:1319–28. https://doi.org/10.1093/nar/gks1222.
67. Alfano D, Franco P, Stoppelli MP. Modulation of cellular function by the urokinase receptor signalling: a mechanistic view. Front Cell Dev Biol. 2022. https://doi.org/10.3389/fcell.2022.818616. (Frontiers Media S.A).
68. Martínez-Hernández MG, Baiza-Gutman LA, Castillo-Trápala A, Armant DR. Regulation of proteinases during mouse peri-implantation development: urokinase-type plasminogen activator expression and cross talk with matrix metalloproteinase 9. Reproduction. 2011;141:227–39. https://doi.org/10.1530/REP-10-0334.
69. Appeltant R, Somfai T, Maes D, Van Soom A, Kikuchi K. Porcine oocyte maturation in vitro: role of cAMP and oocyte-secreted factors-A practical approach. J Reprod Dev. 2016;62(5):439–49.
70. López-Saucedo J, Paramio-Nieto MT, Fierro R, Piña-Aguilar RE. Intracytoplasmic sperm injection (ICSI) in small ruminants. Anim Reprod Sci. 2012. p. 129–38. https://doi.org/10.1016/j.anireprosci.2012.07.003.
71. Kim Y, Kim EY, Seo YM, Yoon TK, Lee WS, Lee KA. Function of the pentose phosphate pathway and its key enzyme, transketolase, in the regulation of the meiotic cell cycle in oocytes. Clin Exp Reprod Med. 2012;39:58–67. https://doi.org/10.5653/cerm.2012.39.2.58.
72. Zhai Y, Yu H, An X, Zhang Z, Zhang M, Zhang S, et al. Profiling the transcriptomic signatures and identifying the patterns of zygotic genome activation – a comparative analysis between early porcine embryos and their counterparts in other three mammalian species. BMC Genomics. BioMed Central Ltd; 2022;23. https://doi.org/10.1186/s12864-022-09015-4.
73. Bohrer RC, Coutinho ARS, Duggavathi R, Bordignon V. The incidence of DNA double-strand breaks is higher in late-cleaving and less developmentally competent porcine embryos. Biol Reprod. Society for the Study of Reproduction; 2015;93. https://doi.org/10.1095/biolreprod.115.130542.
74. Beld J, Lee DJ, Burkart MD. Fatty acid biosynthesis revisited: Structure elucidation and metabolic engineering. Mol. Biosyst. Royal Society of Chemistry; 2015. p. 38–59. https://doi.org/10.1039/c4mb00443d.
75. Wang X, Yu H, Gao R, Liu M, Xie W. A comprehensive review of the family of very-long-chain fatty acid elongases: structure, function, and implications in physiology and pathology. Eur J Med Res BioMed Central Ltd; 2023. https://doi.org/10.1186/s40001-023-01523-7.
76. Samiec M. Molecular mechanisms of somatic cell cloning and other assisted reproductive technologies in mammals: which determinants have been unraveled thus far?—current status, further progress and future challenges. Int J Mol Sci. 2024. https://doi.org/10.3390/ijms252413675. (Multidisciplinary Digital Publishing Institute (MDPI)).
77. Sirithanakorn C, Cronan JE. Biotin, a universal and essential cofactor: synthesis, ligation and regulation. FEMS Microbiol Rev. 2021. https://doi.org/10.1093/femsre/fuab003.
78. Bao B, Rodriguez-Melendez R, Wijeratne SSK, Zempleni J. Biotin regulates the expression of holocarboxylase synthetase in the miR-539 pathway in HEK-293 cells. J Nutr. 2010;140:1546–51. https://doi.org/10.3945/jn.110.126359.

Publisher's Note

Springer Nature remains neutral with regard to jurisdictional claims in published maps and institutional affiliations.